LBL-17304
c2

Lawrence Berkeley Laboratory
UNIVERSITY OF CALIFORNIA

Materials & Molecular Research Division

RECEIVED
LAWRENCE
BERKELEY LABORATORY
APR 17 1984
LIBRARY AND
DOCUMENTS SECTION

ELECTRONIC DEGREES OF FREEDOM IN CLASSICAL MECHANICS

D.P. Ali
(Ph.D. Thesis)

October 1983

TWO-WEEK LOAN COPY
This is a Library Circulating Copy which may be borrowed for two weeks. For a personal retention copy, call Tech. Info. Division, Ext. 6782.

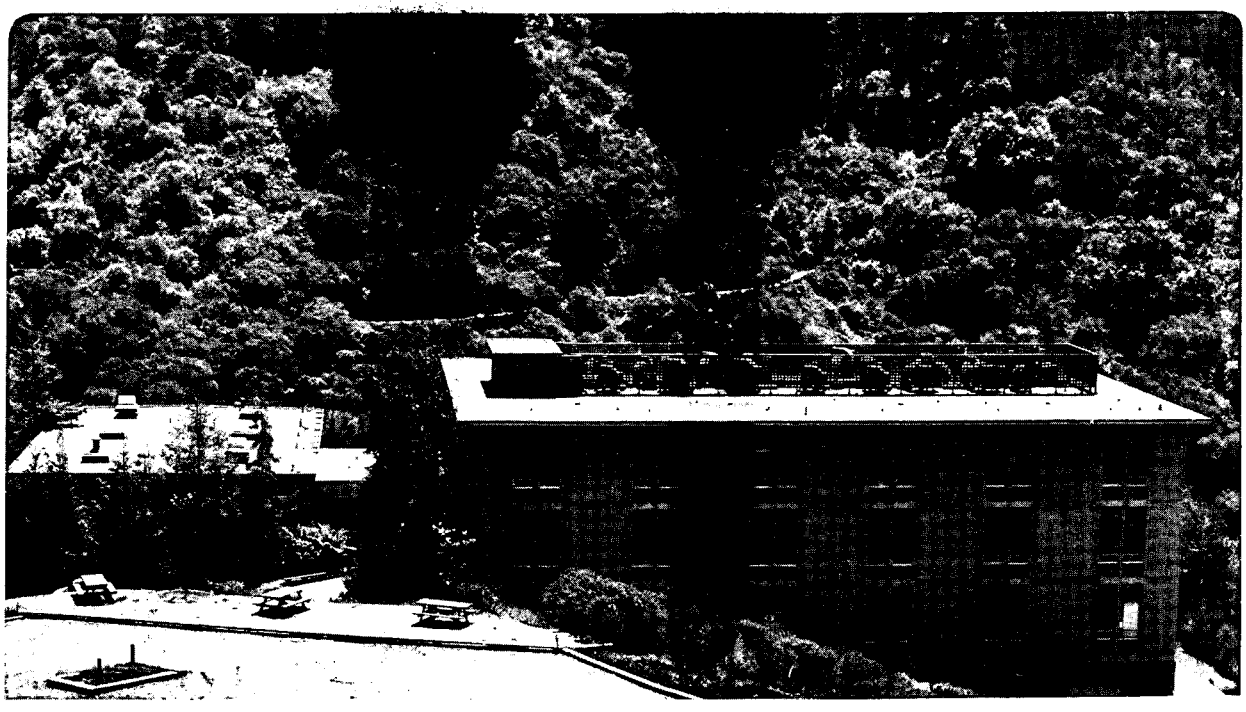

Prepared for the U.S. Department of Energy under Contract DE-AC03-76SF00098

LBL-17304

DISCLAIMER

This document was prepared as an account of work sponsored by the United States Government. While this document is believed to contain correct information, neither the United States Government nor any agency thereof, nor the Regents of the University of California, nor any of their employees, makes any warranty, express or implied, or assumes any legal responsibility for the accuracy, completeness, or usefulness of any information, apparatus, product, or process disclosed, or represents that its use would not infringe privately owned rights. Reference herein to any specific commercial product, process, or service by its trade name, trademark, manufacturer, or otherwise, does not necessarily constitute or imply its endorsement, recommendation, or favoring by the United States Government or any agency thereof, or the Regents of the University of California. The views and opinions of authors expressed herein do not necessarily state or reflect those of the United States Government or any agency thereof or the Regents of the University of California.

LBL-17304

ELECTRONIC DEGREES OF FREEDOM IN CLASSICAL MECHANICS

Domenic Paul Ali
(Ph.D. Thesis)

Materials and Molecular Research Division
Lawrence Berkeley Laboratory
University of California
Berkeley, CA 94720

October 1983

This work was supported by the National Science Foundation under Grant CHE-79-20181 and by the Director, Office of Energy Research, Office of Basic Energy Sciences, Chemical Sciences Division of the U.S. Department of Energy under Contract No. DE-AC03-76SF00098.

ELECTRONIC DEGREES OF FREEDOM

IN

CLASSICAL MECHANICS

Domenic Paul Ali

ABSTRACT

Electronic degrees of freedom are generally considered purely a quantum mechanical phenomenon not treatable within the framework of classical mechanics. In this dissertation, we show the above statement not to be true. In the first part of the dissertation, a classical analog for electronic degrees of freedom developed by Miller [JCP 72, 2272(1980)] is shown to correctly describe Stükelberg oscillations and electronic-vibrational and rotational resonance phenomenon, strictly quantum mechanical processes, within a classical Hamiltonian framework. In the second part of the dissertation, a semiclassical model for electronic transitions developed by Miller and George [JCP 56, 5637(1972)] is coupled with both a Langevin model and a Generalized Langevin model and shown to correctly describe electronic dynamics in iodine recombination in a solvent. The results obtained are in good agreement with experiment.

ACKNOWLEDGEMENTS

First and foremost, I wish to express my gratitude to Professor Miller for his patience in always answering my questions and for his understanding of my rebellious nature. I would also like to thank NRCC for supplying the coupled channel code and L. Thomas for his help in implementing it; R. Kapral, G. Schatz and L. Pratt for many enlightening discussions on statistical mechanics; S.A. Adelman for graciously supplying the frequency parameters.

I most importantly wish to thank Renee Contratto and Dan Rubinate for always doing their best to make my life a joy. And, of course, Theresa De Sabatto. This work was supported by the National Science Foundation under Grant CHE-79-20181 and by the Director, Office of Energy Research, Office of Basic Energy Sciences, Chemical Sciences Division of the U.S. Department of Energy under Contract Number DE-AC03-76SF00098.

TABLE OF CONTENTS

	Page
Abstract	1
Acknowledgements	i
Introduction	1
Part A: Electronic Transitions in Reactions Occuring in the Gas Phase	3
I. The Ehrenfest Model	4
II. Stückelberg Oscillation Model Problem	10
III. Collinear $Br^* + H_2$	14
IV. Classical Analog Model for F^*, $Br^* + H_2$ in 3-Dimensions	21
V. Ehrenfest Model Conclusion	35
Part B: Electronic Transitions in Reactions Occuring in Liquids	42
VI. Iodine Recombination: Introduction	43
VII. The Surface Hopping Langevin Trajectory Model	46
VIII. The Generalized Langevin Model	59
IX. Iodine Recombination: Conclusion	72
References	73
Tables	80
Figure Captions	84
Figures	87

You enumerate Its laws and in my thirst for knowledge I admit that they are true. You take apart its mechanism and my hope increases. At the final stage you teach me that this wondrous and multi-colored universe can be reduced to the atom and that the atom itself can be reduced to the electron. All this is good and I wait for you to continue. But you tell me of an invisible planetary system in which electrons gravitate around a nucleus. You explain this world to me with an image. I realize then that you have been reduced to poetry: I shall never know. Have I the time to become indignant?

Albert Camus

Introduction

Twenty-five years ago, Ford and Wheeler showed that elastic atom-atom scattering could be described semiclassically. Since then, a whole field has developed to describe the collisions of atoms and molecules using classical and semiclassical mechanics. During the first twenty years, all effort went into describing heavy particle motion, i.e., translations, rotations and vibrations, with these techniques and discovering their limitations with respect to quantum mechanics. It was believed during this period that electron motion could never be described classically, and, so electronic states could never be described classically, i.e., electronic transitions. Some attempts were made to surmount this problem in the early '70's (such as the Tully-Preston[18] surface hopping model), but the models presented were not completely satisfactory. Today, I believe the situation to be different. It is not only possible to describe electronic transitions classically, but one can describe purely quantum mechanical resonance phenomenon using only classical Hamiltonian mechanics. The first part of this thesis explores this question with a model developed by Miller.[21-25]

The second part of the thesis moves away from the gas phase into solution chemistry and shows that one can successfully combine a Langevin model, a purely classical model, with the Miller-George theory of electronic transitions, a semiclassical model, to describe the dynamics of a recombination reaction involving ten electronic surfaces. I hope to convince the reader that electronic transitions

can be described within a classical framework and, particularly in the recombination process, give results that are theoretically unobtainable by any other fashion.

PART A: ELECTRONIC TRANSITIONS IN REACTIONS OCCURING IN THE GAS PHASE

I. The Ehrenfest Model.

Gas phase collision theory has seen a great surge of interest in the application of classical and semiclassical mechanics to molecular reactions in the last twenty-five years. These methods have been applied to a wide variety of problems involving translational, rotational, and vibrational degrees of freedom with much success. Excellent reviews of semiclassical[1,2] and classical[3,4] techniques as applied to molecular collisions are now available.

As collisions on one Born-Oppenheimer surface using non-quantum techniques are becoming better understood (i.e., collisions involving only heavy particle degrees of freedom), attention has been turning to non-adiabatic collisions. These types of reactions are observed in a great number of fundamental molecular processes[5-15] such as electronic energy transfer, charge transfer, quenching of electronic excitation and chemical reactions. In the spirit of non-quantum approaches to molecular collisions, semiclassical theories have been developed which treat the electronic degrees of freedom quantum mechanically and the heavy particle degrees of freedom classically. The many variants of the Landau-Zener model[20] are in this general category, such as the Miller-George theory[17] and the Tully-Preston surface hopping model.[18] It has been pointed out,[19] however, that such models may miss important dynamical features since part of the system is being treated classically and part quantum mechanically. This problem is particularly pronounced in electronic-vibrational and electronic-rotational resonance energy transfer. The obvious solution to this is to treat the whole problem on the same dynamical footing. Since treating the system quantum mechanically is

computationally unfeasible for many-body problems, we are left with a complete classical description of the collision system as the only alternative.

Several attempts of this type have been recently tried.[21-30] In the opinion of this author, Meyer and Miller's Ehrenfest model[25] has shown the most promise. We will therefore concentrate on the Ehrenfest model in the hope of determining what the limitations of this model are and how well the results from this model compare with quantum mechanical calculations.

We begin by considering a collision system having F electronic states, for which the quantum mechanical Hamiltonian operator is

$$H_Q = \frac{\underset{\sim}{p}^2}{2\mu} + \sum_{kk'}^{F} |k\rangle\, V_{kk'}(\underset{\sim}{x})\, \langle k'| \tag{1}$$

where $\underset{\sim}{x}$ denotes the coordinates of all the heavy particle degrees of freedom and $\underset{\sim}{p}$ their conjugate momenta. $V_{kk'}(\underset{\sim}{x})$ are the diabatic matrix elements of the interaction potential. To solve this problem classically, we must find a classical analog for H_Q, specifically we must find a classical analog for the potential matrix $\underset{\approx}{V}(\underset{\sim}{x})$.

In the Ehrenfest model, we begin by looking at the expectation value of the potential function

$$V_{CL}(\underset{\sim}{x}) \equiv \langle\psi(t)|\underset{\approx}{V}(\underset{\sim}{x})|\psi(t)\rangle \tag{2}$$

where $|\psi(t)\rangle$ is the electronic wavefunction of our system. If we expand the wavefunction into the electronic basis set $|k\rangle$,

$$|\psi(t)\rangle = \sum_k C_k(t)|k\rangle \tag{3}$$

then we have

$$V_{CL}(\underset{\sim}{x}) = \sum_{kk'} C_k^*(t)\ C_{k'}(t)\ V_{kk'}(\underset{\sim}{x}) \tag{4}$$

with $V_{kk'}(\underset{\sim}{x})$ being the same matrix elements defined in Eq. (1). $C_k(t)$ satisfy the usual first-order time dependent equation

$$C_k(t) = -i \sum_{k'} V_{kk'}(\underset{\sim}{x})\ C_{k'}(t). \tag{5}$$

If we now define new real variables n_k, q_k such that

$$C_k(t) \equiv \sqrt{n_k(t)}\ e^{-iq_k(t)}$$

and substitute this into Eq. (4), we obtain

$$V_{CL}(\underset{\sim}{x},\underset{\sim}{n},\underset{\sim}{q}) = \sum_{kk'} \sqrt{n_k n_{k'}}\ e^{i(q_k - q_{k'})}\ V_{kk'}(\underset{\sim}{x})\ . \tag{6}$$

Thus our classical analog to the quantum Hamiltonian of Eq. (1) is

$$H_{CL}(\underset{\sim}{x},\underset{\sim}{p},\underset{\sim}{n},\underset{\sim}{q}) = \frac{\underset{\sim}{p}^2}{2\mu} + V_{CL}(\underset{\sim}{x},\underset{\sim}{n},\underset{\sim}{q})$$

For example, with two electronic states and the fact that $n_0 + n_1 = 1$ (conservation of probability), our classical analog reduces to

$$H_{CL}(\underset{\sim}{x},\underset{\sim}{p},n,q) = \frac{p^2}{2\mu} + n\, V_{11}(\underset{\sim}{x}) + (1-n)\, V_{00}(\underset{\sim}{x})$$

$$+ 2\sqrt{n(1-n)}\, V_{01}(\underset{\sim}{x}) \cos q \tag{7}$$

where we have assumed that $V_{01}(\underset{\sim}{x})$ is real.[118] If we momentarily ignore the last term in Eq. (7), we see that the potential the system feels is an average of the diabatic curves weighted by the probability of being on electronic surface $|0\rangle$ or $|1\rangle$. This is the initial common sense guess we might make if trying to construct this model <u>ad hoc</u>. The last term in Eq. (7) takes into account the coupling $V_{01}(\underset{\sim}{x})$. Note that if the coupling $V_{01}(\underset{\sim}{x})$ were zero, then H_{CL} would be q-independent and therefore n becomes a conserved quantity. We therefore see that our classical model satisfies all the qualitative requirements we expect of it.

This model is intimately connected with Ehrenfest theorem[31] which states that

$$\frac{d}{dt}\langle p\rangle = \frac{i}{\hbar}\langle[H,p]\rangle = -\langle\psi(t)|\frac{\partial H(t)}{\partial x}|\psi(t)\rangle$$

$$\frac{d}{dt}\langle x\rangle = \frac{i}{\hbar}\langle[H,x]\rangle = \langle\psi(t)|\frac{\partial H}{\partial p}|\psi(t)\rangle \tag{8}$$

It is easily shown[25] that Eq. (7) and Eq. (8) are equivalent if we determine H(t) from $H(\underset{\sim}{x}(t))$ in Eq. (8). The classical analog model is therefore similar to the semiclassical models[32] where a classical trajectory is chosen, $\underset{\sim}{x}(t)$, and then the evolution of the electronic state $|\psi(t)\rangle$, is determined by solving Eq. (5) with the predetermined

heavy particle trajectory. The Ehrenfest model allows the trajectory to be determined from the evolution of the electronic state. One would therefore imagine that this model should give a more accurate representation of the dynamics than those models where we pre-determine $\underset{\sim}{x}(t)$. Since this model is basically a semiclassical approach to electronic transitions we expect that it should have all the advantages and disadvantages inherent in the semiclassical approach.[33]

It is important to note that the Ehrenfest model does not try to follow the trajectory of the electrons, something which classical mechanics clearly cannot do. Rather, it follows the motion of the <u>pattern of electron motion</u>, a motion much slower than electron motion and therefore amiable to treatment with classical mechanics. This point should be kept in mind for otherwise the reader may form the incorrect opinion that classical mechanics correctly describes electron motion.

Two additional analog models, the spin matrix method (SMM)[23] and the classical pseudopotential (CPP)[24] have been developed by Miller, <u>et al.</u> In the SMM, the potential matrix $\underset{\approx}{H}$ is expanded in a spin basis set, $\underset{\approx}{S}_x$, $\underset{\approx}{S}_y$, $\underset{\approx}{S}_z$ and the spin matrices are equated with the classical components of the spin vector. In the CPP model a complete Hamiltonian for the collision system is constructed, nuclei plus electrons. The electronic degrees of freedom that do not change during the collision are then averaged over and the remaining electronic degrees of freedom are equated to the electronic potential functions. All three methods give the same classical Hamiltonian for two electronic surfaces but differ for three or more. I have chosen the Ehrenfest model over the others for two reasons. First, only the Ehrenfest model allows us to

make a connection with the quantum equations of motion for the evolution of C(t), Eq. (5). While this is not absolutely necessary, it is aesthetically pleasing to be able to do so. Second, and more important, a unitary transformation of $\underset{\approx}{H}$ quantum mechanically corresponds to a canonical transformation of the $(\underset{\sim}{n},\underset{\sim}{q})$ variables classically. The Ehrenfest model is the only one of the three which exhibits this property of basis set independence. I therefore feel that the Ehrenfest model is the more appropriate one of the three to use in actual calculations. This will be borne out in our FH_2 calculations below.

II. Stückelberg Oscillation Model Problem.

We begin our investigation of the Ehrenfest model with an application to a collinear collision between two structureless particles with two electronic surfaces. Such a system will give rise to Stückelberg oscillations[34] in the S-matrix elements. As mentioned above, the motivation for devising the Ehrenfest model was to treat all the degrees of freedom on the same dynamical footing and correctly model the energy exchange between these modes. In such a system as we have chosen, the predominant dynamical motion is a translational-electronic resonance energy exchange. Such a system will therefore prove useful in answering the question of whether it is possible to describe quantum resonance effects with purely classical mechanics. To enhance the Stukelberg oscillations, we have chosen near-degenerate electronic curves without any additional heavy particle degrees of freedom. We choose as our model the following:

$$
\begin{aligned}
V_{00}(r) &= A\, e^{-\alpha r} \\
V_{11}(r) &= A\left(1-\frac{\Delta}{k}\right) e^{-\alpha r} + \Delta \\
V_{01}(r) &= \gamma\, e^{-(r-r_0)^2/2\sigma^2}
\end{aligned}
\qquad
\begin{aligned}
\Delta &= 1.0\,\text{eV} \\
A &= 83.9\ \text{eV} \\
k &= 1.0\ \text{eV} \\
\gamma &= 0.2\ \text{eV} \\
\sigma &= 0.4
\end{aligned}
\tag{9}
$$

and r_0 chosen at the crossing point of V_{00} and V_{11}. V_{01} was localized as a Gaussian to assure the presence of Stückelberg oscillations. Figure 1 shows the potential curves for the case of $\alpha=2$. The larger α is, the more degenerate the curves are in the coupling region.

The quantum mechanical Hamiltonian for the system is

$$H = \frac{-1}{2\mu} \frac{d^2}{dr^2} \begin{pmatrix} 1 & 0 \\ 0 & 1 \end{pmatrix} + \begin{pmatrix} V_{00} & V_{01} \\ V_{01} & V_{11} \end{pmatrix} \tag{10}$$

The quantum calculations are carried out using a standard couple channel -matrix code obtained from NRCC.[35] We refer the reader to this reference for further details if interested.

The classical Hamiltonian for the system is

$$H(p,r,n,q) = \frac{p^2}{2\mu} + V_{CL}(r,n,q) \tag{11}$$

where $V_{CL}(r,n,q)$ for the two state case is as given in Eq. (7). We carry out the standard quasiclassical procedure[37] to determine the S-matrix elements for the Hamiltonian. Briefly, we choose initial conditions

$$p = -\sqrt{2\mu\ E_{tr}}$$

$$r = \text{large}$$

$$n = 0$$

$$q = 2\pi\ \xi$$

where ξ is a random number between 0 and 1. These conditions put the particles on the V_{00} curve out in asymptopia approaching each other with total energy E_{tr}. We let the system propagate by way of Hamilton's equations of motion

$$\dot{p} = -\frac{\partial H}{\partial r} \qquad \dot{n} = -\frac{\partial H}{\partial q}$$

$$\dot{r} = \frac{\partial H}{\partial p} \qquad \dot{q} = \frac{\partial H}{\partial n}$$

until the particles once again are in the asymptotic region. We then "box" the final n values as

$$-\frac{1}{2} \leq n_f \leq \frac{1}{2} \qquad \text{no transition}$$

$$\frac{1}{2} \leq n_f \leq \frac{3}{2} \qquad \text{transition}$$

The final transition probability for a given energy is then given by

$$P_{2\leftarrow 1}(E) = \frac{1}{2\pi} \int_0^{2\pi} dq \quad h(n_f(E,q) - \frac{1}{2})$$

where h(x) is the heavyside step function. The above is evaluated using the Monte Carlo technique.[39] It was found that 50 trajectories were sufficient to stabilize the results to within 10%. Microscopic reversibility (starting with initial value of n=1 and reversing the boxing procedure) was found accurate to within statistical error.

Results

Figures 2-4 present the results for three different values of α (three different degrees of degeneracy). Figure 2, the most degenerate case, shows excellent agreement between the quasi-classical and quantum results. As the curves become less degenerate, we see that in Figures 3 and 4 the classical calculations reproduce the oscillations with less accuracy. We see that the quasiclassical results average out the quantum oscillations for these latter cases.

We can understand this behavior if we take a closer look at the assumptions of the classical model. As we said earlier, the classical analog model is the usual semiclassical model in which we take the

heavy particle trajectory to be that determined by the Ehrenfest Theorem and is therefore subject to the general restrictions which apply to semiclassical models. Delos, Thorson, and Knudson[33] have found that, among other restrictions, the semiclassical model for electronic transitions requires that the potential surface difference ΔV be small compared to the total energy of collision so that the trajectories on different surfaces don't differ drastically. The extreme case is that of two degenerate potential curves where the trajectories are identical. In such a case, the semiclassical model obtains the correct result.[36] As α becomes smaller, the curves become less and less degenerate and our frequency oscillations in Figure 2 is a Stukelberg oscillation which the classical model correctly predicts. We can therefore say that the classical analog correctly determines quantum interference effects if the potential curves do not differ greatly. In situations where the potential curves do differ substantially, the classical model only determines the average behavior of the S-matrix elements. This model is therefore still very useful for these situations since in general, we always average over some degrees of freedom, such as rotations or vibrations, which average out the quantum interference effects. For example, the model can probably be successfully applied in determining the probability of charge transfer in molecules where there is usually a large difference between electronic surfaces if the vibrational and rotational degrees of freedom are averaged over. On the other hand, the model would not be appropriate in determining the probability of charge transfer between atoms where there are no internal degrees of freedom to average over.

III. Collinear $Br^* + H_2$.

We continue our investigation of the Ehrenfest model with an application to the well-known[40-43] electronic-vibrational energy transfer reaction

$$Br^*(^2P_{1/2}) + H_2(v=0) \rightarrow Br(^2P_{3/2}) + H_2(v=1)$$

This reaction is thought to be[40] a mechanism which efficiently quenches spin-orbit excited Br because the vibrational quantum of H_2 approximately matches the 3685 cm^{-1} excitation energy of Br. This fact is borne out by the quantum mechanical results for the collinear version of this reaction by Lee, et al.[44] This reaction is of interest to us for two main reasons. First, the Br^* quenching involves a resonant energy transfer between electronic and vibrational coordinates. This example will thus allow us to see how the Ehrenfest model does when we include internal degrees of freedom. Second, the coupling between the two electronic states is exponential compared to our first example where it was Gaussian. While in the first case it would have been possible to use a Landau-Zener model to determine the transition probability, this second case spreads the coupling region over a broader region making the transition "more quantum mechanical". It is clearly important to see how our classical model does in such a case.

We will compare our results to those of Lee et al.[40] amd thus follow their formulation of the problem. We treat the H_2-Br system collinearly with H_2 as a simple harmonic oscillator with no rotations

allowed. We treat the potential interaction in two parts. The first part is a non-diagonal spin-orbit interaction matrix while the second is an exponential diagonal matrix representing the electronic interaction (Secrest-Johnson[45] type)

$$\begin{pmatrix} V_{00} & V_{01} \\ V_{10} & V_{\pm 1} \end{pmatrix} = \begin{pmatrix} \frac{1}{3}\lambda & \frac{\sqrt{2}}{3}\lambda \\ \frac{\sqrt{2}}{3}\lambda & \frac{2}{3}\lambda \end{pmatrix} + e^{-\alpha(R - \frac{1}{2} r - \rho_0)} \begin{pmatrix} A_0 & 0 \\ 0 & A_1 \end{pmatrix} \tag{12}$$

In this representation, transitions between the two states are due solely to the spin-orbit interaction. Here V is the vibrational coordinate, R is the translational coordinate, and λ is the spin-orbit splitting. A_0, A_1, ρ, and λ are parameters chosen to resemble the Br-H_2 system. The values for these constants are reported elsewhere.[46]

While this form of $\underline{\underline{V}}$ is correct, one notes that in the asymptotic region ($R \to \infty$), we still have finite off-diagonal elements, so that we will still have transitions in the asymptotic region for this choice of adiabatic states. This situation is easily alleviated by performing a unitary transform on $\underline{\underline{V}}$ such that we diagonalize the spin-orbit interaction. This is easily done and we find

$$\begin{pmatrix} V'_{00} & V'_{01} \\ V'_{10} & V'_{11} \end{pmatrix} = \begin{pmatrix} 0 & 0 \\ 0 & 1 \end{pmatrix} + e^{-(R - \frac{1}{2} r - \rho_0)} \begin{pmatrix} A_{00} & A_{01} \\ A_{10} & A_{11} \end{pmatrix} \tag{13}$$

with

$$A_{00} = \frac{2}{3} A_0 + \frac{1}{3} A_1$$

$$A_{11} = \frac{2}{3} A_1 + \frac{1}{3} A_0$$

$$A_{01} = A_{10} = \frac{\sqrt{2}}{3} (A_1 - A_0)$$

With this set of diabatic states, we see that $\underline{\underline{V}}'$ is diagonal as $R \to \infty$. We now replace the interaction matrix, $\underline{\underline{V}}'$, with our classical model for electronic degrees of freedom, Eq. (7)

$$V'_{CL}(R,r,n,q) = e^{-\alpha(R - \frac{1}{2} r - \rho_0)} [n A_{11} + (1-n) A_{00}] + n\lambda + 2\sqrt{n(1-n)} \cos q \, A_{01} \tag{14}$$

with n,q being the action-angle variables representing the electronic states described previously. Letting $R \to \infty$, we find

$$V'_{CL}(R \to \infty, r, n, q) = n\lambda$$

which is independent of q so that n is a conserved quantity in the asymptotic region. (This was our motivation for the unitary transformation). Since n=0,1 represents the ground and excited spin-orbit state respectively, we see that asymptotically we remain in a given spin orbit state.

Given this functional form for the interaction matrix, we can easily write down the Hamiltonian

$$\mathcal{H}(p,R,v,q_v,n,q) = \frac{p^2}{2\mu} + (v+\frac{1}{2})\omega + V'_{CL}(R,r,n,q) \tag{15}$$

where P is the translation momentum, ω is the H_2 frequency, and v is the action variable for the oscillator. To complete this description, we must refine the vibrational coordinate r in terms of the action angle variable v,q_2. This is easily done and known to be[47]

$$r = r_0 + \sqrt{\frac{2v+1}{m\omega}} \cos q_v$$

with r_0 the equilibrium position of the vibrator and m the reduced mass of the oscillator. The values used for r_0, m and μ are given elsewhere.[46]

With the Hamiltonian defined, we need only implement Hamilton's equations of motion and define the initial conditions. Beginning with H_2 in its ground vibrational state and Br in its spin orbit excited state we have

$$\begin{aligned} P &= \sqrt{2\mu\ E_{tr}} \\ R &= \text{large} \\ v &= 0 \\ q_v &= q \\ n &= 1 \\ q &= \xi \end{aligned} \qquad 0 \leq \xi \leq 2\pi$$

where E_{tr} is the translational energy and ξ is a random number between 0 and 2π as usual.

To extract the final quantum probabilities from the classical trajectories, we will use two different methods. The first is the histogram method[37] described in the first example where we box the final values of v and n as shown in Figure 5. Another procedure used less frequently is the moment method[48,49] in which one determines the first and higher moment of $\langle\Delta V\rangle$ and $\langle\Delta N\rangle$ as well as the correlation moments $\langle\Delta V\ \Delta N\rangle$ using quantum probabilities. One can then invert these equations to solve for the probabilities in terms of the moments. To determine the quantum transitions, we then calculate these moments <u>classically</u> via a Monte Carlo procedure.[39]

$$\langle\Delta N^{\alpha}\ \Delta V^{\beta}\rangle = \int_0^{2\pi} dq \int_0^{2\pi} dq_v\ (n_f-n_i)^{\alpha}\ (V_f-v_i)^{\beta} \tag{16}$$

In determining the equations for the moments, one must determine how many vibrational states one wishes to include since including different numbers of vibrational states will give different results. It would seem that the states to be included should be those which are classically populated and indeed this was found to give the best agreement with the quantum mechanical results. With the given initial conditions, it was found that v = 0,1,2 were populated along with n=0,1. Including these six states in the inversion formula, we find for example that the resonant probability is

$$\begin{aligned} P_{\substack{v=1,n=0\\ \leftarrow v=0,n=1}} &= \langle\Delta n\ \Delta v\ (\Delta v-2)\rangle \\ &= \int_0^{2\pi} dq \int_0^{2\pi} dq_v\ (n_f-n_i)(v_f-v_i)(v_f-v_i-2) \end{aligned} \tag{17}$$

with similar equations for the other transition probabilities.

Results

So as to compare to the results of Lee, et al.,[44] we did calculations with v=1, n=0 as the initial state. Figures 6 and 7 are plots of the resonant quenching probability as a function of the artificially varied spin-orbit splitting using both the moment method and the histogram method. Exact resonance occurs at $\lambda = 0.02$ a.u. We see that the histogram method gives qualitatively correct results with the resonance peak produced in the proper place. The moment method on the other hand gives excellent quantitative agreement with the quantum results to within 5%.

The remaining plots have been done with v=0 and n=1 for the initial conditions since this is the physically interesting direction, the quenching of Br^*. Figures 8 and 9 include both the resonant and non-resonant quenching probability for two additional energies using the moment method. While we do not have quantum results to compare to here, we note that the resonant probability has a single peak which becomes sharper with lower translational energy and that the non-resonant probability is large when the energy miss match between the vibrational energy spacing and the spin-orbit splitting is large (for small λ) dropping to zero at resonance. These are the results one would expect and in lieu of the agreement for Figures 6 and 7 with the quantum results, we have an equal amount of confidence in these plots as well.

The most interesting of these graphs is Figures 9 which is in the thermal energy region at $\sim$ 0.6 kcal/mole. We see here that the resonant peak is very sharp, so sharp that if one looks at the physical value of λ = 0.0167 a.u., we see that the resonant effect is negligible. Thus from the collinear results, one would conclude that the resonant effect is only predominant at energies higher than thermal. Figure 10 is a conventional plot of probability vs. energy for the physical value of λ. Here we see that the resonant curve peaks peaks at 0.04 a.u., well above thermal energies, while the non-resonant curve is basically zero (except for some numerical fluctuations). We will have more to say about this in the next section.

IV. Classical Analog Model for F^*, $Br^* + H_2$ in 3D.

In the examples studied so far, the Ehrenfest model has proven to be of sufficient accuracy to merit an application to a three-dimensional system. We will therefore apply our model to electronic quenching of F^* and Br^* by H_2. The quenching of Br^* will thus be extended to include H_2 rotation, and orbital and total angular momentum. Before looking at the full BrH_2 system, it will prove useful to examine the rotational-electronic resonance reaction

$$F^*(^2P_{1/2}) + H_2 \rightarrow F(^2P_{3/2}) + H_2^{\dagger}$$

This reaction is one of the few which has been simple enough to determine the three-dimensional quantum cross section[50-52] so that we may compare our results to. More importantly is that this reaction has also been studied classically by Meyer and Miller[23] using the SMM discussed above. As we said earlier, the three different analog models, the CPP, the SMM, and the Ehrenfest model do not give the same form for the classical potential for more than two electronic states. Since the FH_2 system involves three electronic states,[23] we should therefore be able to determine which of the two models, SMM or the Ehrenfest, is the more correct to use. We will then examine the BrH_2 system and compare our three-dimension results to the collinear results above.

To begin our derivation of the FH_2 Hamiltonian, we take as our starting point the classical Hamiltonian derived by Meyer and Miller for the SMM model.[23]

$$\mathcal{H} = \frac{p^2}{2\mu} + \frac{\ell^2}{2mR^2} + B_{rot}\, N^2 + B_j{}^2 + V_{CL}(R,\gamma,m_L,q_{m_L}) \tag{18}$$

where the first two terms are the translational kinetic energy, the third and forth terms are the rotational and spin-orbit energy, respectively, and the last term is the SMM classical function for the electronic matrix. The electronic matrix $\underline{\underline{V}}$ is the Lester-Rebentrost surfaces[50] rotated from their original cartesian basis set to a polar basis set[23] (ℓ=1, m_i=-1,0,1)

$$\underline{\underline{V}} = \begin{pmatrix} H & \frac{i}{\sqrt{2}} H_{yz} & -\Delta \\ -\frac{i}{\sqrt{2}} H_{yz} & H_{zz} & -\frac{i}{\sqrt{2}} H_{yz} \\ -\Delta & \frac{i}{\sqrt{2}} H_{yz} & \bar{H} \end{pmatrix} \tag{19}$$

It is this matrix which is modeled by the SMM classical function. It should be pointed out that the above Hamiltonian is assuming a rigid rotator for H_2. The reader is referred to the Meyer-Miller paper for further details.[23] In deriving Eq. (18), the electronic matrix was put into the $|\ell,m_L\rangle$ basis set because this appeared to be the most logical choice. On the other hand, the spin orbit interaction term is in the $|j,m_j\rangle$ basis. While there is nothing that strictly forbids us doing this for a classical Hamiltonian, it would be preferred that these two terms have the same basis set for reasons soon to be seen.

There are several ways to do this, but we have chosen the following: make a unitary transformation of $\underline{\underline{V}}$ from $|\ell,m_L\rangle$ to the

$|j,m_j\rangle$ basis. Rewrite the spin-orbit term back into matrix notation. The advantage of doing this is that we may now add these two matrices and obtain the complete electronic-spin orbit matrix. <u>We then model this full matrix with the Ehrenfest model</u>.

To do this, we first note that we can no longer work with the 3 x 3 matrix of Eq. (19), but must expand it to a 6 x 6 to include both projections of electron spin for the F atom. We must do this for otherwise we would have an incomplete basis set for a unitary transformation to the $|j,m_j\rangle$ basis. Our V matrix is therefore

$$\underset{\approx}{V} = \begin{pmatrix} \bar{H} & \frac{i}{\sqrt{2}} H_{yz} & -\Delta & 0 & 0 & 0 \\ -\frac{i}{\sqrt{2}} H_{yz} & H_{zz} & -\frac{i}{\sqrt{2}} H_{yz} & 0 & 0 & 0 \\ -\Delta & \frac{i}{\sqrt{2}} H_{yz} & \bar{H} & 0 & 0 & 0 \\ 0 & 0 & 0 & \bar{H} & \frac{i}{\sqrt{2}} H_{yz} & -\Delta \\ 0 & 0 & 0 & -\frac{i}{\sqrt{2}} H_{yz} & H_{zz} & -\frac{i}{\sqrt{2}} H_{yz} \\ 0 & 0 & 0 & -\Delta & \frac{i}{\sqrt{2}} H_{yz} & \bar{H} \end{pmatrix} \tag{20}$$

with the order of the basis set being $|m_\ell,m_j\rangle = |-1,-1/2\rangle$, $|0,-1/2\rangle$, $|1,-1/2\rangle$, $|-1,1/2\rangle$, $|0,1/2\rangle$, $|1,1/2\rangle$. The 3 x 3 blocks in this matrix are Eq. (19). We now perform a unitary transformation to the coupled representation

$$|m_L\ m_S\rangle \underset{\underset{\approx}{U}}{\rightarrow} |j,\ m_j\rangle$$

where $\underset{\approx}{U}$ in the usual transformation matrix derived from the Clebsch-Gorden coefficients.[53] Our new matrix is

$$\underset{\approx}{H}_{e\ell} = \underset{\approx}{U}^{\dagger} \underset{\approx}{V} \underset{\approx}{U} \tag{21}$$

where $\underset{\approx}{H}_{e\ell}$ is in the $|j,m_j>$ basis. The results of this algebra are presented in Appendix A. We next write the spin-orbit term in its matrix representation. In the $|j,m_j>$ basis, the matrix is diagonal with the elements

$$H^{SO}_{jm_j,j'm_j'} = B\ j(j+1)\ \delta_{jj'}\ \delta_{m_j\ m_j'} \tag{22}$$

where B is the spin-orbit constant.

We finally add the electronic and spin-orbit matrices to get the composite electronic-spin orbit Hamiltonian $\underset{\approx}{H}^T$

$$\underset{\approx}{H}^T = \underset{\approx}{H}^{SO} + \underset{\approx}{H}^{e\ell}$$

One then need only apply Eq. (6) to our matrix $\underset{\approx}{H}^T$

$$\begin{aligned}
\underset{\approx}{H}^T(\underset{\sim}{n},\underset{\sim}{q},R,\gamma) = {} & (n_1+n_4)\bar{H} + (n_2+n_3)\underset{\sim}{H} \\
& + (n_5+n_6)\underset{\sim}{H}^{-1} + (n_1+n_2+n_3+n_4)3B \\
& + 2\sqrt{\tfrac{2}{3}}\,\Delta\,[\sqrt{n_1n_6}\cos q_6 - \sqrt{n_5n_4}\cos(q_5-q_4)] \\
& + 2\sqrt{\tfrac{1}{3}}\,\Delta\,[\sqrt{n_1n_3}\cos q_3 - \sqrt{n_2n_4}\cos(q_4-q_2)] \\
& + 2\,H\,[\sqrt{n_2n_5}\cos(q_5-q_2) - \sqrt{n_6n_3}\cos(q_6-q_3)]
\end{aligned}$$

$$+ \sqrt{2}\, H_{yz}\, [\sqrt{n_6 n_2}\, \cos(q_6 - q_2) - \sqrt{n_5 n_3}\, \cos(q_5 - q_3)]$$

$$+ 2\sqrt{\tfrac{1}{3}}\, H_{yz}\, [\sqrt{n_2 n_1}\, \cos q_2 - \sqrt{n_4 n_3}\, \cos(q_4 - q_3)]$$

$$+ 2\sqrt{\tfrac{1}{6}}\, H_{yz}\, [\sqrt{n_6 n_4}\, \cos(q_6 - q_4) - \sqrt{n_5 n_1}\, \cos q_5)] \tag{23}$$

where (n,q) are the action-angle variables representing the six quantum states. All other variables are defined in Appendix A. Due to conservation of probability, we can always eliminate one of the n's in favor of the other five so that H^T is only a function of five pairs of action-angle variables. It is H^T, for example, that gets diagonalized to find the electronic surfaces for FH_2 with the spin-orbit term included. It is because the reaction is occuring on these surfaces, rather than just the electronic ones that we believe it is better to treat the spin-orbit term as part of the matrix to be modeled classically. We could also have left $H^{e\ell}$ in its original basis set and performed the unitary transformation on H^{so} of course, but since the asymptotically interesting states are the $|j,m_j>$ one, we have chosen the latter. The reader is reminded that one of the virtues of the Ehrenfest model is that different basis sets for the matrix correspond to different canonical variables so that one obtains the same results with this Hamiltonian, independent of basis set. This is not true of the SMM where one must decide the more "physically meaningful" basis set to use. This is the major appeal of the Ehrenfest model.

To complete the description of the Hamiltonian, we must still represent the orbital angular momentum, $\underset{\sim}{\ell}$, in the centrifugal term

in terms of the other independent angular momentu. This has been previously done,[21] but we quickly outline the derivation. There are four angular momenta, J, the total, ℓ, the orbital, N, the rotational and j the coupled angular momentum. Due to convervation, we know

$$\underset{\sim}{J} = \underset{\sim}{\ell} + \underset{\sim}{j} + \underset{\sim}{N} \tag{24}$$

so that

$$\ell^2 = J^2 + j^2 + N^2 + 2\underset{\sim}{j}\cdot\underset{\sim}{N} - 2\underset{\sim}{J}\cdot\underset{\sim}{j} - 2\underset{\sim}{J}\cdot\underset{\sim}{N} \tag{25}$$

by a few simple algebraic manipulations, we can get this in the form

$$\ell^2 = (J^2+N^2) + (j^2-2j_z^2) + 2j_x(N_x-J_x) + 2j_y(N_y-J_y) - 2\underset{\sim}{J}\cdot\underset{\sim}{N} \tag{26}$$

As usual, we can express J vector in its action angle variables (J,q_J), (m_J,q_{m_J})[47]

$$\begin{aligned} J_z &= m_J \\ J_y &= \sqrt{J^2-m_J^2}\ \sin q_{m_J} \\ J_x &= \sqrt{J^2-m_J^2}\ \cos q_{m_J} \end{aligned} \tag{27}$$

with similar expressions for N. The point of this exercise is that we cannot do the same for j since it is no longer represented as an action-angle pair, but as part of the H^T matrix. We must therefore

write the matrix expressions for j and its components and then apply the Ehrenfest model to these as well. For example, in the $|j,m_j>$ basis

$$j_z = \frac{1}{2}\begin{pmatrix} 3 & & & & & \\ & 1 & & & & \\ & & -1 & & & \\ & & & -3 & & \\ & & & & 1 & \\ & & & & & -1 \end{pmatrix} \tag{28}$$

is the matrix representation for j_z. Applying the Ehrenfest model to this we get

$$j_z = [\frac{3}{2} - (n_2+n_5) -2(n_3+n_6) - 3n_4) \tag{29}$$

where we have eliminated n_1 in favor of the other variables in conservation. This expression gives the average, $|j_z>$, given the distribution among the electronic states. Similar expressions for the other components along with j,j^2 are presented in Appendix B. Together with Eq. (29), we now have an expression for ℓ^2 in terms of the independent variables of our total Hamiltonian. For the sake of completeness, it is presented here.

$$H(R,P,N,\ell,\underset{\sim}{n},\underset{\sim}{q},\gamma) =$$

$$\frac{p^2}{2\mu} + \frac{\ell^2}{2\mu R^2} + B_{rot}N^2 + H^T(\underset{\sim}{n},\underset{\sim}{q},R,\gamma) \tag{30}$$

with ℓ given by (A.8) in Appendix B and H^T given by Eq. (23).

Given Eq. (30), we carried out our calculations within the framework of the standard quasiclassical trajectory model. The Langer modification[38] was made to all action variables

$$J \to J + \frac{1}{2} \qquad N \to N + \frac{1}{2} \qquad \underset{\sim}{n} \to \underset{\sim}{n} + \frac{1}{2} \tag{31}$$

The cross section for $(j_1,N_1) \to (j_2,N_2)$ transition was summed over m_{N_2},m_{j_2} and averaged over m_{N_1},m_{j_1} and is given by[23]

$$\sigma_{j_2N_2 \leftarrow j_1N_1} = \frac{\pi}{K^2_{j_1N_1}} \sum (2J+1) \quad \bar{P}_{j_2N_2 \leftarrow j_1N_1}(J)$$

where ($\hbar$ = 1)

$$K_{j_1N_1} = \sqrt{2\mu \; E_{j_1N_1}}$$

and E_{j,N_1} is the translational energy with respect to the $|j_1N_1\rangle$ state.

We have calculated $\bar{P}_{j_2N_2 \leftarrow j_1N_1}$ in three ways. The first is the standard histogram procedure similar to that used for the collinear BrH_2 computation where we have boxed our final results as in Figure 11. The second method is that of skewed histogram[23] method used by Meyer and Miller in which we skew the boxes so that they lie in the direction of the resonance line also shown in Figure 11. It was found that this skewing gave more reasonable results for the resonant and nonresonant channels. The third method used to determine $\bar{P}_{j_2N_2,j_1N_1}$ was the moment method in which we include j = 1/2,3/2 and up to N=0,2,4 (recall that H_2 is homonuclear and only the even rotational

states are populated). All integrals involved were evaluated by the usual Monte Carlo method.[37,39]

FH_2 Results

We will be predominantly interested in the (1/2,0) → (3/2,2) resonant transition which has an energy defect of 6.2 meV. As found by Meyer and Miller the skewed histogram procedure gave larger resonant cross sections and sections and smaller non-resonant cross sections [(1/2,0) → (3/2,0)] than the histogram proceedure. The moment method gave similar results to the skewed histogram proceedure for the resonant cross section, but gave non-resonant cross sections comparable to the resonant cross sections. Lester and Rebentrost[52] determine the non-resonant cross section to be an order of magnitude smaller than the resonant. This is in contrast to the collinear H_2Br calculation where we found the moment method to give the best results.

As with the SMM calculations, microscopic reversibility for the resonant cross section is poorly obeyed. We thus follow Meyer and Miller and define an average cross section[23]

$$\bar{\sigma} = \sqrt{\sigma \cdot \hat{\sigma}}$$

where σ is the cross section calculated from the intial state (1/2,0) and $\hat{\sigma}$ the cross section calculated from the intial state (3/2,2) and then corrected for the degeneracy effect. In lieu of the above discussion, we have only presented $\bar{\sigma}$ for the skewed histogram proceedure in figure 12.

We see that while the SMM results give the correct order of magnitude, they do not reproduce the resonant peak at 20 meV. The Ehrenfest results, on the other hand, predict a resonance peak at 40 meV. The opacity function, plotted in figure 13, for E_T = 60 meV shows that while both the SMM and Ehrenfest results are too small compared to the quantum, the Ehrenfest calculation predicts a resonance peak, whereas, the SMM calculation shows no resonance structure in P(b). Figures 12 and 13 allow us to conclude, therefore, the Ehrenfest model can correctly predict the resonance structure in both the cross section and opacity function though it does underestimate them by a factor of two. We also see that it is essential to have the Hamiltonian basis-set consistent to reproduce the resonant energy exchange.

BrH_2

Our second three-dimensional reaction is the electronic-vibrational resonance of spin orbit excited Bromine with H_2 in its ground vibrational state. The spin orbit splitting in Bromine is 3685 cm^{-1} and so is more closely akin to the vibrational level space of H_2 which is 4161 cm^{-1}, almost an order of magnitude greater than the FH_2 defect. We would therefore expect this resonance to occur, if at all, at higher energies than that of FH_2 and expect it to be much broader.

Our main concern here is generating potential surfaces which are more reliable than the model ones used for the collinear case. We have chosen to use the DIM approach for its simplicity and ease. We have followed a procedure completely analogous to that of Tully's[54,55] used to generate the FH_2 surface where we have simply replaced the FH $\Sigma^{1,3}$ and $\Pi^{1,3}$ states by those of BrH. The Σ curves were obtained from Porter and Raft[56] while the $\Pi^{1,3}$ curves were calculated via a SCF calculation.[57] Even though SCF is not of great accuracy, we feel that for our purposes it will suffice. We found the transition state for this surface to lie 24.9 kcal/mole above the Br + H_2 channel which compares relatively well with the experimentally measured value of 19.7.[58] Since the resonance energy exchange will take place completely in the entrance channel, the saddle point discrepancy is not a serious problem.

In solving the DIM matrix, we must diagonalize a 24 x 24 matrix (which blocks out into smaller parts) to obtain the adiabatic curves. Unfortunately, we cannot use these curves in our classical Hamiltonian as written since we are assuming diabatic states which contain the coupling within the potential matrix. The adiabatic representation contains the coupling within the kinetic energy terms, i.e., it is no longer diagonal. While we could do the calculation this way, we would need to calculate the kinetic energy coupling terms along with the adiabatic surfaces along with writing a different program than that used for FH_2. There is an approximate though much easier way around this. We can perform a partial diagonalization of the DIM matrix to diagonalize out the spin, but leave the spacial components of the basis set unaltered. This leaves us with an approximate

diabatic matrix in the cartesian basis set. Since this was the original basis set we used for the FH_2 calculation, we can simply replace the potential functions. The derivatives for these potentials needed for Hamilton's equations are determined by finite differences. We now use the Hamiltonian of Eq. (23) with one final modification. This is an electronic-vibrational energy transfer, so we can no longer treat H_2 as a rigid rotor. We must add a kinetic energy term for the H_2 vibration and the diabatic states will also depend on r, the H_2 inter-nuclear distance, B_{rot} is no longer constant but

$$B_{rot} \rightarrow \frac{1}{2\mu\ r^2}$$

where μ is the reduced mass of H_2. With these additions, our Hamiltonian now becomes

$$\mathcal{H}(P,R,p,r,\ell,N,\underset{\sim}{n},\underset{\sim}{q},\gamma) =$$

$$\frac{p^2}{2m} + \frac{\ell^2}{2\mu\ R^2} + \frac{p^2}{2} + \frac{N^2}{2\mu\ r^2} + H^{\tau}(\underset{\sim}{n},\underset{\sim}{q},\underset{\sim}{R},\underset{\sim}{r},\gamma)$$

We now follow the standard quasiclassical trajectory model as we did with FH_2 except that we are interested in the vibrational transition instead of the rotational. The procedure and equations are the same as FH_2 so they will not be repeated.

BrH_2 Results

Before going on to discuss the results, there are some practical points of the calculation that need mention. The BrH_2 calculations

take an exceeding long time to carry out for several reasons. First, since H_2 is vibrating, the integration steps in our integrator must be made very small so as to be comparable with the H_2 vibrational period. Second, unlike FH_2, we no longer have analytic expressions for the potential surfaces. We must diagonalize a 2 by 2 and partial diagonalize a 4 by 4 <u>each time</u> we take a step with our integrator. Third, we must determine the three gradients of the potential surfaces by finite differences. The combination of these lead to very long CPU times, especially for the low translational energies so that we are severely limited to the number of cross sections we can evaluate. Because of this, we have not done a geometrical average to correct for the microscopic irreversibility as we did for FH_2. Rather, we have calculated the cross sections using the skewed histogram procedure alone since this method of extracting the final quantum numbers gave the best results in the FH_2 case. Judging from FH_2, we can say that the BrH_2 results as calculated will probably be qualitatively similar to what we would have calculated if we had done a geometric average of the cross sections. Figure 14 has a plot of the cross sections for the resonant ($v=0$, $j=1/2 \rightarrow v=1$, $j=3/2$) and nonresonant ($v=0$, $j=1/2 \rightarrow v=0$, $j=3/2$) channels as a function of translational energy. We have chosen the ground rotational and vibrational state of H_2 and the spin-orbit excited state of Br as the initial state. We did not thermally average over the initial rotational state since it was found that different initial rotational states gave the same cross sections within statistical error. From Figure 14, we see that the resonant cross section has an upward trend toward smaller translational energies. It does not appear that this cross section has a single peak as did

the FH_2 case. One can not be too definitive about this since the uncertainties are so large. Unfortunately, we could not run more than 1000 trajectories to reduce the uncertainties since the CPU time needed would have been unreasonable. The non-resonant cross section is seen to be much smaller than the resonant cross section as we would have expected.

While we have no direct experimental evidence to compare to, we note that Leone et al.[59] have recently determined the rate constant for resonant energy transfer for this reaction and found the thermally averaged cross section at room temperature to be 0.3 $\mathring{A}^2$. Figure 14 qualitatively agrees with these experimental results and does show the resonant cross section to be an order of magnitude greater than the non-resonant. Due to numerical difficulties, we cannot say anything more quantitative than this.

Comparing our results to the H_2Br collinear calculation discussed above, we see they are vastly different. The collinear results show a definite resonance at 0.04 hartrees while the three-dimensional calculations show the cross section exponentially decreasing as a function of energy. This discrepancy implies that the probability that comes from impact parameters other than b=0 play a substantial role in determining the cross section for this system. As always, one must view collinear calculations with great suspicion when comparing to experimental situations.

V. Ehrenfest Model Conclusions

We have shown that it is possible to model electronic states, a purely quantum mechanical phenomenon, with classical mechanics and obtain results which are in good agreement with quantum mechanical calculations. In particular we have shown that the Ehrenfest model can correctly describe the major energy transfer reactions; electronic-vibrational, electronic-rotational, and electronic-translational. Of the two models, the SMM and the Ehrenfest model, the latter has been shown to give better agreement with quantum mechanics for three or more states.

In conclusion, the Ehrenfest model has been shown to give semi-accurate results if the electronic states do not differ much and the general semiclassical conditions are observed.

Appendix

A. We start with Eq. (20)

$$V=\begin{bmatrix} \bar{H} & \frac{i}{\sqrt{2}}H_{yz} & -\Delta & & & \\ -\frac{i}{\sqrt{2}}H_{yz} & H_{zz} & \frac{i}{\sqrt{2}}H_{yz} & & & \\ -\Delta & \frac{i}{\sqrt{2}}H_{yz} & \bar{H} & & & \\ & & & H & \frac{i}{\sqrt{2}}H_{yz} & -\Delta \\ & & & -\frac{i}{\sqrt{2}}H_{yz} & H_{zz} & \frac{i}{\sqrt{2}}H_{yz} \\ & & & - & \frac{i}{\sqrt{2}}H_{yz} & \bar{H} \end{bmatrix} \tag{A.1}$$

We must now perform a unitary transformation from the uncoupled to coupled representation

$$|j\ m_j\rangle = \underset{\approx}{U}|m_L, m_S\rangle \tag{A.2}$$

The transformation matrix is the usual Clebsh-Gorden coefficients[23] and is easily calculated as

$$\underset{\approx}{U} = \begin{pmatrix} 0 & 0 & 0 & 0 & 1 & 0 \\ 0 & 0 & a & 0 & 0 & g \\ g & 0 & 0 & a & 0 & 0 \\ 0 & 1 & 0 & 0 & 0 & 0 \\ 0 & 0 & -g & 0 & 0 & a \\ -a & 0 & 0 & g & 0 & 0 \end{pmatrix} \tag{A.3}$$

with $g = \sqrt{1/3}$ and $a = \sqrt{1/2}$.

We find $\underset{\approx}{H}^{e\ell} = \underset{\approx}{U}\underset{\approx}{V}\underset{\approx}{U}^{+}$ to be

$$H_{e\ell} = \begin{bmatrix} \bar{H} & \underset{\sim}{H}_{yz} & -\underset{\sim}{\Delta} & 0 & -\underset{\sim}{H}_{yz}^{-1} & \underset{\sim}{\Delta}^{-1} \\ -\underset{\sim}{H}_{yz} & \underset{\sim}{H} & 0 & -\underset{\sim}{\Delta} & H & \frac{i}{2} H_{yz} \\ -\Delta & 0 & \underset{\sim}{H} & -\underset{\sim}{H}_{yz} & -\frac{i}{2} H_{yz} & -H \\ 0 & -\underset{\sim}{\Delta} & \underset{\sim}{H}_{yz} & \bar{H} & \underset{\sim}{H}_{yz} & -\underset{\sim}{\Delta} \\ H_{yz}^{-1} & H & \frac{i}{2} H_{yz} & -\underset{\sim}{\Delta}^{-1} & \underset{\sim}{H}^{-1} & 0 \\ \underset{\sim}{\Delta}^{-1} & -\frac{i}{\sqrt{2}} H_{yz} & -H & -\underset{\sim}{H}_{yz}^{-1} & 0 & \underset{\sim}{H}^{-1} \end{bmatrix} \tag{A.4}$$

where

$$\underline{H} = \frac{2}{3} H_{zz} + \frac{1}{3} H \qquad \underset{\sim}{H}_{yz}^{-1} = \frac{i}{\sqrt{6}} H_{yz}$$

$$\underset{\sim}{H}^{-1} = \frac{2}{3} H + \frac{1}{3} H_{zz} \qquad \underset{\sim}{\Delta}^{-1} = \sqrt{\frac{2}{3}}$$

$$\underset{\sim}{H}_{yz} = \frac{i}{\sqrt{3}} H_{yz} \qquad \underset{\sim}{H} = \frac{\sqrt{2}}{3} (\bar{H} - H_{zz})$$

$$\underset{\sim}{\Delta} = \frac{i}{\sqrt{3}} \Delta$$

We need only add the spin orbit interaction matrix (Eq. 22)

$$\underset{\approx}{H}^{SO} = \begin{pmatrix} 5 & & & & & \\ & 5 & & & & \\ & & 5 & & & \\ & & & 5 & & \\ & & & & 1 & \\ & & & & & 1 \end{pmatrix} \frac{3}{4} B \tag{A.5}$$

to $H_{e\ell}$ to obtain H^T. Substitution of H^T into Eq. (6) gives us the Ehrenfest model expression of H^T, Eq. (23).

B. To determine our expressions for j and its projections, we begin with the matrix form of these operators

$$j_x = \frac{1}{2}\begin{bmatrix} 0 & \sqrt{3} & 0 & 0 & & \\ \sqrt{2} & 0 & 2 & 0 & & \\ 0 & 2 & 0 & \sqrt{3} & & \\ 0 & 0 & \sqrt{3} & 0 & & \\ & & & & 0 & 1 \\ & & & & 1 & 0 \end{bmatrix} ; \; j = \frac{1}{2}\begin{bmatrix} \sqrt{15} & & & & & \\ & \sqrt{15} & & & & \\ & & \sqrt{15} & & & \\ & & & \sqrt{15} & & \\ & & & & \sqrt{3} & \\ & & & & & \sqrt{3} \end{bmatrix}$$

$$j_y = \frac{i}{\sqrt{2}}\begin{bmatrix} 0 & -\sqrt{3} & 0 & 0 & & \\ \sqrt{3} & 0 & -2 & 0 & & \\ 0 & 2 & 0 & \sqrt{3} & & \\ 0 & 0 & \sqrt{3} & 0 & & \\ & & & & 0 & -1 \\ & & & & 1 & 0 \end{bmatrix} ; \; j^2 = \frac{1}{4}\begin{bmatrix} 15 & & & & & \\ & 15 & & & & \\ & & 15 & & & \\ & & & 15 & & \\ & & & & 3 & \\ & & & & & 3 \end{bmatrix} \tag{A.6}$$

We then use the Ehrenfest expression for the matrices and find the functional forms to be

$$j_x = \sqrt{3}\ [\sqrt{n_1 n_2}\ \cos q_2 + \sqrt{n_3 n_4}\ \cos(q_4 - q_3)] + 2\sqrt{n_1 n_3}\ \cos(q_3 - q_2) + \sqrt{n_5 n_6}\ \cos(q_6 q_5)$$

$$j_y = -\ [\sqrt{3}(\sqrt{n_1 n_2}\ \sin q_2 + \sqrt{n_3 n_4}\ \sin(q_4 - q_3) + 2\sqrt{n_2 n_3}\ \sin(q_3 - q_2) + \sqrt{n_5 n_6}\ \sin(q_6 - q_5)$$

$$j = \frac{1}{2}\ [\sqrt{15} + (n_5 + n_6)(\sqrt{3} - \sqrt{15})$$

$$j^2 = \frac{1}{4}\ (15 - (n_5 + n_6)12) \tag{A.7}$$

Using these expressions and Eq. (26) and Eq. (29), we find our expression for ℓ^2, the orbital angular momentum to be

$$\ell^2 = (J^2 + N^2) + (j^2 - 2_{jz}^2) + 2_{jx}\ (\sqrt{N^2 - m_N^2}\ \cos q_m - \sqrt{J^2 - m_J^2})$$

$$+ 2_{jy}\ (\sqrt{N^2 - m_N^2}\ \sin q_{m_N})$$

$$- 2(m_J m_N + \sqrt{J^2 - m_J^2}\ \sqrt{N^2 - m_N^2}\ \cos q_{m_N}) \tag{A.8}$$

c. Following Tully's procedure[54] for the construction of the DIM matrix, we have a 6 x 6 block matrix out of the full 24 x 24 matrix which is relevant to the three lowest adiabatic states

$$\mathcal{H}^{DIM} = \begin{bmatrix} H_{11} & H_{12} & H_{13} & H_{14} & & \\ & H_{22} & H_{23} & H_{24} & & \\ & & H_{33} & H_{34} & & \\ & & & H_{44} & & \\ & & & & H_{55} & H_{56} \\ & & & & & H_{66} \end{bmatrix}$$

which further block diagonalizes to a 2 x 2 and a 4 x 4. The basis set for this matrix is

$$|y;\tfrac{1}{2},\tfrac{1}{2}\rangle, \quad |y;\tfrac{1}{2},\tfrac{1}{2}\rangle, \quad |z;\tfrac{1}{2},\tfrac{1}{2}\rangle, \quad |z;\tfrac{1}{2},\tfrac{1}{2}\rangle, \quad |x;\tfrac{1}{2},\tfrac{1}{2}\rangle, \quad |x;\tfrac{1}{2},\tfrac{1}{2}\rangle$$

where the spacial part of the basis set is in the cartesian representation while the spin part represents the total coupled spin of all the atoms and its projection. The two by two block is composed of only the x-spatial component so that in diagonalizing it, we end up with two adiabatic surfaces of solely x character. The lower of these two surfaces corresponds to H_{xx} of Eq. (19).

The 4 x 4 block has both y and z spacial components so that if we diagonalize this block we will mix the y and z components. We would like to keep the spacial components unmixed so that we will have a cartesian diabatic basis set, but one would like to diagonalize out the spin component. An approximate way to do this would be to diagonalize the 4 x 4 block as follows

$$\begin{bmatrix} C & -S & & \\ S & C & & \\ & & \underline{C}' & -\underline{S}' \\ & & \underline{S}' & \underline{C}' \end{bmatrix} \cdot \begin{bmatrix} H_{11} & H_{12} & H_{13} & H_{14} \\ & H_{22} & H_{23} & H_{24} \\ & & H_{33} & H_{34} \\ & & & H_{44} \end{bmatrix} \cdot \begin{bmatrix} C & S & & \\ -S & C & & \\ & & \underline{C}' & \underline{S}' \\ & & -\underline{S}' & \underline{C}' \end{bmatrix}$$

$$= \begin{bmatrix} H'_{11} & 0 & H'_{13} & H'_{14} \\ 0 & H'_{22} & H'_{23} & H'_{24} \\ & & H'_{33} & 0 \\ & & 0 & H'_{44} \end{bmatrix} \qquad \begin{matrix} c' = \cos\gamma & c = \cos\theta \\ s' = \sin\gamma & s = \sin\theta \end{matrix}$$

where we have diagonalized the yy block and the zz block. Ideally, we would like the yz blocks to also be diagonal after the unitary transformation. Though this is not rigorously true, we have found that the yz block were approximately diagonal. Taking the smaller of the diagonal elements from each block we have a 2 x 2 diabatic matrix in the yz basis set. We have found that for a H_2 -Br distance greater than 1.5 Å, the partial diagonalization technique yields potential surfaces that are within a kcal/mole of the full diagonalization (the usual method). For H_2Br distances less than 1.5 Å the discrepancy increases to 4 kcal/mole. This is well into the saddle point region though and our trajectories do not sample this region at all; all resonant energy exchange takes place in the entrance channel. We therefore feel that this partial diagonalization is an adequate approximation.

PART B: ELECTRONIC TRANSITIONS IN REACTIONS OCCURING IN LIQUIDS

VI. Iodine Recombination: Introduction.

In the first part of this thesis, we showed that is was possible to describe electronic transitions in gas phase collisions using only classical mechanics. We next turn our attention to the description of the electronic dynamics of reactions occuring in liquids. Unlike the gas phase, we cannot follow all the relevant heavy particle degrees of freedom exactly (there being of the order of 10^{23}) so that we must do a statistical approach to this part of the problem. For example, the method we have chosen to follow is a Langevin approach where we follow the exact dynamics of the reacting atoms and treat the solvent atoms as a heat bath. The reacting atoms are allowed to exchange energy with the bath thru a systematic and random force. This greatly simplifies the number of heavy particle degrees of freedom which we must follow.

Since the inclusion of electronic degrees of freedom for reactions occuring in liquids is still in its infancy, it is best to focus on the simplest possible reaction where electronic states are known to play a significant role in the dynamics. Iodine recombination in liquids is such a reaction. Since the first experimental results on this system were obtained in 1961 by Noyes,[60] and extensive interest has developed in the study of this as well as other recombination reactions. Iodine recombination has been studied in a variety of solvents[61-65,73] and there have also been a number of experimental[66-68] and theoretical[68-70] studies of the process in the gas phase. Of particular importance are the picosecond experiments[61-65,73] which allow one to study the short time scale inherent in this reaction.

Since recombination is perhaps the simplest "chemical reaction"

that one can study in liquids, it has attracted considerable theoretical attention. Studies have included molecular dynamics simulations[61-63] and stochastic trajectory,[64-65] or Langevin approaches. While molecular dynamics is relatively common nowadays, the computational effort involved is considerable in following the specific dynamics of each individual particle in the system. The Langevin approach is much easier to employ and can describe longer time behavior, but it incorporates many more approximations whose validity is difficult to ascertain. There are thus many fundamental theoretical questions about the dynamics of recombination in liquids that merit further investigation.

The present work follows closely the Langevin stochastic trajectory model of Hynes, Kapral, and Torrie,[64] where the focus is on <u>secondary recombination</u>[66] of the iodine atoms; i.e., one considers the iodine atoms that, after photo-excitation of I_2, have separated to a distance of $\sim$ 4-6 Å, from which they either recombine (on a time scale of $\sim$ 10-30 picoseconds) or dissociate permanently. (<u>Primary</u> recombination of the atoms immediately after the excitation takes place within a picosecond and is typically obscured by the exciting laser pulse.) In their Langevin simulation Hynes, <u>et al.</u>, considered motion of iodine atoms only on the ground electronic potential curve of I_2, although they noted that the other electronic states which dissociate to ground state iondine atoms should also be taken into account. Figure 15 shows the ten diatomic potential curves of I_2 that arise from two $^2P_{3/2}$ iodine atoms,[67] and one sees that at $\sim$ 4-6 Å they are all within kT of each other, suggesting that electronic transition between them should be facile in this region.

Previous work dealing with the question of electronic transitions in iodine recombination includes that of Bunker,[68] who discussed it only on statistical grounds, and that of Martire and Gilbert,[75] who used a Folker-Planck equation which included rate constants for transitions between the various electronic states of I_2. In their actual calculations Martire and Gilbert assumed only one electronically excited state, and the rate of transitions between it and the ground state was varied in order to obtain agreement with experiment. While this was a good start of dealing with the effects of electronic transitions, one would like to have a less phenomenological approach that is also tractible enough to allow practical calculations.

We have decided to follow the Langevin stochastic trajectory approach of Hynes, et al., but generalize it to incorporate the effects of electronic transitions between the various potential curves (i.e., electronic states) of I_2. Specifically, we utilize the Tully-Preston surface-hopping model[78] to allow for localized "hops" from one potential curve to another, with the electronic transition probability determined by the generalized Stückelberg model of Miller and George. Since the surface-hopping model is formulated in a probabilistic framework--i.e., a "hop" from the current electronic state is made or not by comparing the electronic transition probability to a random number--it is relatively easy to include it in the stochastic trajectory simulation.

VII. The Surface Hopping Langevin Trajectory Model.

We begin by discussing the Langevin model[83] and some basic aspects pertinent to iodine recombination. As mentioned above, the Langevin model only follows the dynamics of the primary atoms (i.e., iodine atom) in detail and treats the solvent atoms as a "bath". The equation of motion for each iodine atom is

$$m_i[d\underset{\sim}{v}_i(t)/dt] = -\xi_i \underset{\sim}{v}_i(t) + \underset{\sim}{F}_i(t) + \underset{\sim}{R}_i(t) \qquad (i=1,2) \tag{32}$$

Here m_i is the iodine atomic mass, $\underset{\sim}{F}_i = -\underset{\sim}{\nabla}_i V(r)$ is the iodine potential interaction, ξ_i the frictional constant, $\underset{\sim}{R}_i(t)$ the gaussian-distributed random force, and $\underset{\sim}{v}_i(t)$ the iodine atom velocity for atom i. The frictional term slows the iodine atoms down while they move through solvent while the random force represents the momentum transfer to and from the solvent. Rigorously, the partitioning of the solvent-solute interaction into systematic and random components is only a conceptual aid. This is seen by the fact that ξ_i and $\underset{\sim}{R}_i(t)$ are related by the second fluctuation-dissipation theorem[81]

$$2\,\xi_i(t)\,\delta_{ij} = \langle \underset{\sim}{R}_i(t)\cdot\underset{\sim}{R}_j(0)\rangle$$

which insures that the primary atoms remain in thermal equilibrium with the bath.

Deutch and Oppenheim[80] have shown that Eq. (32) can be derived from the full solvent-solute system if the following two assumptions

are valid: 1) rapid solvent equilibration compared to solute velocity equilibration, and 2) neglect of intersolute dynamical correlations. The first condition is met if I_2 is immersed in a light solvent (for example, liquid Ar). The second condition can be restated as: the off-diagonal elements of $\underline{\underline{\xi}}$ matrix[88] are small compared to the diagonal elements. While this is not rigorously true, Hynes, et al.,[64] have given a reasonable argument for the neglect of the off-diagonal elements. Under these restrictions, the results we obtain below should be only considered qualitatively correct. We can rearrange Eq. (32) to solve for the relative velocity and coordinate to obtain

$$\mu\left(\frac{d\underline{v}}{dt}\right) = -\xi\, v(t) + F(t) + R(t) \tag{33}$$

where μ is the reduced mass, $v = v_2 - v_1$, $\xi = \frac{1}{2}\xi_1 = \frac{1}{2}\xi_2$, and $R(t) = \frac{1}{2}(R_2(t) - R_1(t))$. Since $\underline{\underline{\xi}}$ is diagonal in our approximation and $F(t)$ is only a function of $r = r_2 - r_1$, we can follow the evolution of Eq. (33) independent of the center of mass equation. We take the friction constant to be[83]

$$\xi = \frac{kT}{2D_0}$$

with D_0 following the temperature dependence

$$D_0(T) = D_0(300)\ (T/300)^{1/2}$$

as given by Enskog theory.[82] We take $D_0(300) = 10^{-5}$ cm^2/sec. The

immediately above two equations and the fluctuation dissipation theorem completely define Eq. (33) except for the potential interaction F(t) which we now discuss.

As noted above, the new aspect of the present work is that we allow the potential function V(r) (i.e., the electronic state) for two iodine atoms to change during the Langevin trajectory according to the surface hopping model.[78] (Hynes, et al., also include in V(r) a "caging potential" which includes the average effect of the solvent on the I-I interaction since its effect is rather small and since our interest here is in investigating the effect of electronic transitions between different I-I potential curves, we ignore this term in the present work). We use the Miller-George semiclassical theory[79] to determine the probability of transition from state i to j. Briefly, this theory extends the Landau-Zener-Stuckelberg electronic transition theory[34,38] for atom-atom collisions to include internal degrees of freedom. Electronic transitions from state i to j are found to be localized at the times when $\Delta V_{ij}(t) = |V_i(t)-V_j(t)|$ passes through a local minimum as a function of t; if t_0 is such a time, then the probability of the i→j transition is given approximately by

$$P_{j\leftarrow i} \simeq \exp[-\frac{4}{3}(\Delta V_{ij}/\hbar)(2\Delta V_{ij}/\Delta\ddot{V}_{ij})^{1/2}] \tag{34}$$

where

$$\Delta V_{ij} = \Delta V_{ij}(t_0)$$

$$\ddot{\Delta V}_{ij} = \frac{d^2}{dt^2} \Delta V_{ij}(t_0)$$

For the present application the potential curves $\{V_i(r)\}$ for the various electronic states (see below for their specific form) are such that

$$|V_i(r) - V_j(r)|$$

is a monotonically decreasing function of r for all i and j; thus $\Delta V_{ij}(t) \equiv \Delta V_j(r(t))$ passes through a local minimum only when r(t) experiences an <u>outer turning point</u>, i.e., when

$$\dot{r}(t_0) = 0 \tag{35a}$$

and

$$\ddot{r}(t_0) < 0 \quad . \tag{35b}$$

This happens whenever the trajectory experiences a sufficient "kick" from the random force that the separating I atoms are turned around and headed back towards each other. Furthermore, this means that a local minimum occurs in $\Delta V_{ij}(t)$ <u>simultaneously</u> for all possible final electronic states j.

The way the surface-hopping model works, therefore, is that one begins in electronic state i, say, and thus integrates the stochastic trajectory, Eq. (33), with $V(r) = V_i(r)$; when r(t) experiences an outer turning point, i.e., Eq. (35) occurs, one calculates the probability (via Eq. (34), and see below) of "hopping" to other electronic states j, and makes a "hop" by comparing these probabilities to random numbers; if a hop is made to electronic state j, then one continues integrating the stochastic trajectory with $V(r) = V_j(r)$, until r(t) experiences another outer turning point, at which point another "hop" is allowed, etc. (It should be noted that this model only allows for electronic transitions which arise from the I-I relative coordinate motion. Transitions induced by solvent collisions are not taken into account (except when they cause an outer turning point in the I-I motion). While these types of transitions are neglected in this calculation, one would expect such transitions to be small for a close shell solvent, such as Ar.)

There is one significant modification we need to make in the above discussion: the transition probability given by Eq. (34) applies to an isolated I-I collision and thus satisfies the relation

$$P_{j\leftarrow i} = P_{i\leftarrow j} \quad . \tag{36}$$

The Langevin model, however, describes the I-I system in interaction with a thermal bath; we thus use Eq. (34) to calculate the probability of de-excitation transitions $i\rightarrow j$, and then invoke <u>detailed balance</u>

to obtain the probabilities of excitation transitions:

$$P_{j\leftarrow i} = (g_j/g_i)P_{i\leftarrow j}\ e^{-\beta(V_j-V_i)} \quad , \tag{37}$$

where $V_i < V_j$ are the electronic energies at the time of transition, and g_i and g_j are the degeneracies of states i and j. Detailed balance has the effect that after many transitions a Boltzmann distribution over the states would result if the energies $\{V_i\}$ were constant. Also, the "primitive" semiclassical transition probabilities given by Eqs. (34) and (37) are not normalized as they stand, i.e., do not satisfy conservation of probability, so they are modified as follows,

$$(P_{j\leftarrow i})_{\text{normalized}} = P_{j\leftarrow i} / \sum_k P_{k\leftarrow i} \quad , \tag{38}$$

in order to do so. One particularly interesting limit of this model to consider is that in which transitions between electronic states are much faster than the relative I-I motion, for all values of r. If this were true, then the electronic states would maintain themselves in a Boltzmann distribution for all values of r, and the effective I-I potential V(r) in the Langevin equation, Eq. (33), would be simply the Boltzmann average of the potential functions $V_i(r)$,

$$\bar{V}(r) = \sum_i g_i V_i(r)\ e^{-\beta V_i(r)} \Big/ \sum_i g_i\ e^{-\beta V_i(r)} \quad . \tag{39}$$

We have thus carried out the Langevin stochastic trajectory

calculation using this average I-I potential function in order to compare it to the resul-s of the surface-hopping model. It is clear that it is much simpler in practice to use one average potential function rather than to deal with the dynamics of transitions between several different potentials, so it is important to see how the results of using this thermally averaged potential compare with those of the more dynamically correct surface-hopping model.

For the potential functions we have been using a standard Morse potential,

$$V_1(r) = De[e^{-2\alpha(r-r_e)} - 2\, e^{-\alpha(r-r_e)}] \quad , \tag{40}$$

with

$$D_e = 5.7144 \times 10^{-2} \text{ hartrees}$$
$$\alpha = 0.98819\ a_0^{-1}$$
$$r_e = 5.03962\ a_0$$

for the ground electronic state, and all the others are described as quadrupole-quadrupole interactions,[77]

$$V_i(r) = C_i/r^5 \quad , \tag{41}$$

$i = 2,\ldots,10$; the constants C_i are given in Table I, along with their symmetry labels and degeneracies. Since we only need to follow the I-I dynamics for $r \geq 4$ Å (see next section), this description of the

excited state potential functions should be a reasonable approximation. Of the ten states, five are repulsive and five attractive.

Finally, we note one simplifying modification we made in carrying out the surface hopping calculations. It was assumed above that $\Delta V_{ij}(r) \equiv |V_i(r)-V_j(r)|$ is a monotonically decreasing function of r for all states i and j, so that $\Delta V_{ij}(t)$ has a local minimum--and thus electronic transitions occur--only at an outer turning point of the r(t) motion. One sees in Figure 15, however, that this is not true if state i or j is the ground electronic state and r > 6 Å. Thus for r > 6 Å there is the possibility of electronic transitions other than at an outer turning point, but we have ignored them in our calculations. While it would certainly have been possible to include them in the surface-hopping description, the results are essentially unchanged by their neglect. This is because electronic transitions are already very facile for r > 6 Å, generating a Boltzmann-like distribution over the electronic states (see next section), so that including even more electronic transitions in this region of r would not change the situation.

Results and Discussion.

The stochastic trajectories are begun at I-I internuclear distance r_0, in electronic state i, with the momentum $\vec{p}$ selected at random from a Boltzmann distribution. We have used two different initial distances r_0 = 5.5 Å and 6.67 Å, to assess this effect on the results, and in addition to T = 300°K have also carried out the calculations for T = 500° and 700°. There is only on a small effect (a few %) on the results of choosing different initial electronic states.

Similar to Hynes et al., we choose inner and outer cut-off points for the trajectory to determine when the iodine atoms have either recombined or permanently separated respectively; these values are 4 Å and 12 Å, respectively. Recombination is said to have occurred, therefore, if r(t) reaches the value 4 Å and the electronic state is the ground state; at this point the iodine atoms are drawn essentially monotonically inward, and the electronic energy gap to other states is sufficiently large that no further transitions occur. Trajectories are followed until r(t) reaches one of these cut-off points, up to a total time of 150 psec; 99% of the trajectories have reached one of the cut-offs by this time timit. Specifics of the numerical integration procedure are discussed by Turq, Lantelme, and Friedman.[84]

Before discussing the major results,it is useful to note that within the present model there is a qualitative correspondence between the collision frequency of I_2 in the liquid and the number of outer turning points that the relative I-I motion experiences (which is also the number of opportunities the I-I system has to make an electronic transition). Thus the collision frequency can be estimated

by[85]

$$Z \simeq Z_g \, g(r) \qquad ,$$

where Z_g is the gas phase collision frequency and g(r) the radical distribution function at contact. Typical values give a collision frequency that varies from ∿ 20 to 30 collisions per picosecond as T varies from 300°K to 700°K, while the average number of outer classical turning points in our stochastic trajectory surface-hopping calculations varies from ∿ 20 to 25 over this temperature range.

Figure 16 shows the principal results of the paper, the probability P(t) that the iodine atoms have not recombined by time t. All three curves result from a Langevin stochastic trajectory calculation, the one labeled G being the result of Hynes, et al., that used the ground state I-I potential curve, that labeled T the result of using the thermally average potential curve, Eq. (39), and that labeled S the result of allowing V(r) to change to the various potentials $\{V_i(r)\}$ according to the semiclassical surface-hopping model. The first qualitative observation is that both curves T and S, which include the effects of electronically excited states, give less recombination, and this is easy to understand: recombination can only take place on the ground state potential, so any transitions out of the ground electronic state will lead to less recombination, i.e., more dissociation.

One sees, however, that the surface-hopping model (curve S) produces a larger correction to the ground state results (curve G) than does use of the thermally averaged potential (curve T); i.e., the surface-hopping model yields even less recombination than does

the thermally averaged potential. This also has a simple explanation: at relatively large values of r, where the potential curves are close together, electronic transitions between the states are facile and do essentially produce a relative Boltzmann distribution among the states, but when r decreases the separation of the ground state potential from the others makes transitions into or out of the ground electronic state improbable; thus the approximate Boltzmann distribution over electronic states at large r is "frozen in" as r decreases, and this means that the surface hopping model produces less population in the ground electronic state at small r than that given by assuming a Boltzmann distribution at small r. With less population in the ground state at small r, the surface hopping model thus gives less recombination than the thermally averaged potential model.

To see more clearly that this interpretation is correct, we show in Figure 17 the average relative population of the different electronic states that results from the surface-hopping calculation (points connected by solid line), compared to a Boltzmann distribution (broken line). Figure 17a is for a region of large r (7-8 Å), and one sees that here the surface-hopping model does indeed produce an essentially Boltzmann distribution over the electronic states; for small r (4-5 Å), however, Figure 17b shows that the surface-hopping model produces much less population in the ground electronic state (state #1) than that given by the Boltzmann distribution at small r. This lack of complete electronic relaxation during the relative I-I motion thus appears to be an important feature in the dynamics of recombination.

The results shown in Figure 16 are for initial separation r_0 = 5.5 Å and temperature T = 300°K. Changing either of these does not change the qualitative natures of these curves nor their positions relative to each other, so that the above discussion concerning the effect of electronic transitions is unchanged. The asymptotic value of P(t), ie.., P(∞), the dissociation probability, does of course depend on r_0 and T. The temperature dependence of P(∞) is shown in Figure 18, and one sees that it is qualitatively the same for the three different cases.

The dependence of P(∞) on r_0 is quite sensitive: increasing r_0 from 5.5 Å to 6.67 Å increases P(∞) by about a factor of 2. This is understandable--i.e., starting the trajectories at larger r leads to larger dissociation probability--but it suggests that if the overall model is to be self-contained, one needs to extend it so that the appropriate initial value of r is determined by the dynamics itself and is not an ad hoc parameter. This limitation is resolved in the next section where we use a generalized Langevin equation to determine the heavy-article motion.

Finally, although comparison of the results of these model calculations with experimental recombination rates is clearly tenuous, it is nevertheless interesting. Hynes, et al., estimate a rate constant of $\sim 4 \times 10^{13}$ cm^3/mole-sec from their calculations using only the ground state I-I potential curve,[74,86] compared to the experimental value of $\sim 1\text{-}2 \times 10^{13}$ cm^3/mole-sec of Troe and co-workers.[87] Hynes, et al., attribute this difference to curve-crossing effects in the I_2 electronic levels. If we crudely relate the rate to the time it takes P(t) to fall to half its asymptotic value, then Figure

2 indicates that the rate given by our surface-hopping model (curve S) would be ∿ 4-5 times slower than that of Hynes, et al. (curve G) and thus roughly the same rate as the experimental value. This is interesting and encouraging, but one should of course not make too much of the actual numerical values.

While there are undoubtedly many limitations of the present model for describing recombination dynamics in liquids, we believe it is realistic enough that the qualitative results of our calculations are meaningful. The most significant of these are that electronically inelastic transitions substantially reduce the rate (and final probability) of recombination and that the character of the electronic dynamics changes during the recombination process. Thus at large r electronic transitions are strong and produce a Boltzmann-like distribution over the various electronic states, but as r decreases electronic relaxation ceases to be complete. There is thus an interesting interplay between the electronically inelastic dynamics and the relative motion of the iodine atoms in interaction with the solvent.

VIII. The Generalized Langevin Model.

We saw in the last section that while the surface hopping Langevin model gave reasonable results, we needed to make several *ad hoc* assumptions such as the initial I_2 relative coordinate and a thermalized velocity distribution. This situation *does not* correspond to the initial experimental conditions.

Experimentally,[61-63] I_2 is excited to the $B(^3\pi_{0+\mu})$ and 1 $U(^1\pi)$ state from the ground state $X(^1\Sigma_g^+)$ with a laser tuned to 5300 Å (see figure 19). The relative oscillator strength for these two transitions is 5.18:1.00.[89] The molecules populating the B state undergo collisional predissociation to the 1U state with a rate constant of $K \cong 0.1$ psec^{-1}.[61] The iodine atoms then separate 5-10 Å where they collide with the solvent cage.[90] It is this cage effect (known as the Frank-Rabinowitch cage phenomenon[90]) which prevents the I_2 molecule from completely predissociating as in the gas phase. In the previous section, we began our trajectories with the assumption that the above events, comprising the first few picoseconds, had occurred. A serious limitation to the Langevin equation is that *it does not model the Frank-Rabinowitch cage phenomenon*, and therefore cannot describe this initial phase of the recombination.

In addition to the inability to describe the cage effect, the Langevin model does not adequately take into account the solvent in which the recombination occurs (except in the very crude manner of a diffusion coefficient). Iodine recombination has been studied in a variety of solvents,[61-65,73] most recently by van den Bergh.[101] The variation in the recombination rates observed in these studies cannot be explained by a difference in the diffusion coefficient

alone. This clearly shows that the recombination process is substantially influenced by more than just the bulk properties of the solvent.

A final limitation of the Langevin model as we use it is its independent treatment of each iodine atom as discussed in the last section. At large separation this approximation is adequate, but clearly fails when the iodine atoms are close, such as the initial phase of the recombination process.

The limitations of the Langevin model are overcome by the Molecular Timescale Generalized Langevin Equation (hereafter called MTGLE) approach developed by Adelman, et al.[91-100] The MTGLE approach starts with the formally exact Generalized Langevin equation[102] and develops a hierarchy of dynamical equations which are mathematically equivalent to a set of coupled harmonic oscillators. These equations have been shown to properly reproduce the cage effect in liquids[98] and vibrational relaxation of a molecule in a liquid.[99] The parameters used in the MTGLE model depend on molecular solvent properties[97,98] in addition to bulk properties of the liquid, and properly take into account the non-independence of the solute atoms. While this approach has limitations, to be discussed below, it properly describes the effects which are of relevance to the initial moments of the recombination process. We next proceed to give a brief overview of the MTGLE approach.

MTGLE: A Brief Overview.

Adelman has written a series of papers[90-100] in addition to two reviews[107,108] of the MTGLE approach to liquids. I wish only to very briefly outline the aspects of the theory which are of relevance to this dissertation. The interested reader is referred to the above two reviews which are well written. We begin with the Langevin equation of the last section:

$$m\ddot{\underline{r}}(t) = \underline{F}(t) - \underline{\underline{\xi}}\,\dot{\underline{r}}(t) + \underline{R}(t) \tag{33}$$

where $\underline{r} = (\underline{r}_0, \underline{r}_1)$ are the coordinates of the two iodine atoms, $\underline{\underline{\xi}}$ the diagonal friction matrix, $\underline{R}(t)$ and $\underline{F}(t)$ the random and interatomic force, respectively. Equation (33) is a more specific form of the Generalized Langevin Equation[103]

$$m\ddot{r}(t) = \underline{F}(t) - \int_0^t \underline{\underline{\beta}}(t-\xi)\cdot\dot{\underline{r}}(\xi)\,d\xi + \underline{R}(t) \tag{42}$$

where

$$\underline{\underline{\xi}} = \int_0^\infty \underline{\underline{\beta}}(t)\,dt$$

The integral in equation (42) depends on the past history of the trajectory and is called the memory kernel.[107] Equation (42) can be shown[80] to be equal to the full many-body Hamiltonian for the complete solvent-solute system and is, therefore, exact. While

equation (42) looks simple, it is deceptive. To determine $\underline{\underline{\beta}}(t)$ requires the full solution of the many-body problem and is, thus, no simpler to solve. If we approximate

$$\underline{\underline{\beta}}(t-\xi) \sim C\ \underline{\underline{\delta}}(t-\xi)$$

then we obtain equation (33). Note $\underline{\underline{\beta}}(t)$ is <u>not</u> diagonal due to the correlation of the motion of the two iodine atoms.

Adelman has shown[107] equation (42) can be written as a hierarchy of equations

$$m\ddot{\underline{r}}(t) = \underline{f}(t) - \underline{\underline{\omega}}_{e_0}^2 \cdot \underline{r}(t) + \underline{\underline{\omega}}_{e_1}^2 \cdot \underline{r}_1(t)$$

$$m\ddot{\underline{r}}_1(t) = - \underline{\underline{\omega}}_{e_1}^2 \cdot \underline{r}_1(t) + \underline{\underline{\omega}}_{c_1}^2 \cdot r(t) + \underline{\underline{\omega}}_{c_2}\ \underline{r}_2(t)$$

$$m\ddot{\underline{r}}_2(t) = - \underline{\underline{\omega}}_{e_2}^2 \cdot \underline{r}_2(t) + \underline{\underline{\omega}}_{c_2}^2 \cdot r_1(t) + \underline{\underline{\omega}}_{c_3}^2 \cdot \underline{r}_3(t)$$

$$\vdots$$

$$m\ddot{\underline{r}}_p(t) = - \underline{\underline{\Omega}}_p^2 \cdot \underline{r}_p(t) + \underline{\underline{\omega}}_{c_p}^2 \cdot \underline{r}_{p-1}(t) - \int_0^t \underline{\underline{\beta}}_p(t-\xi) \cdot \dot{r}_p(\xi)\ d\xi + \underline{f}_{p+1}(t) \qquad (43)$$

Equation (43) needs several comments. Note first the integral term in equation (42) has been expanded into a hierarchy of frequency terms. ($\underline{r}_1$, $\underline{r}_2$, ..., $\underline{r}_n$) are fictitious coordinates which act like coupled harmonic oscillators. Adelman has shown these coordinates

correspond to solvent shell structure around the solute for the case of a harmonic solvent. The frequencies ($\underline{\underline{\omega}}^2_{e_0}$, $\underline{\underline{\omega}}^2_{e}$, $\underline{\underline{\omega}}^2_{e_2}$, ...) are the Einstein frequencies of vibration of the different shells while ($\underline{\underline{\omega}}^2_{c_1}$, $\underline{\underline{\omega}}^2_{c_2}$, $\underline{\underline{\omega}}^2_{c_3}$, ...) are the coupling parameters between adjacent shells. In particular, $\underline{\underline{\omega}}^2_{e_0}$ is the Einstein frequency for the solute atoms in the first shell, while $\underline{\underline{\omega}}^2_{c_1}$ describes the coupling of first shell to the solute, i.e., energy transfer rate between the solvent and solute. Finally, $\underline{\underline{\Omega}}^2_{p}$ is the adiabatic frequency with which the pth shell would vibrate while $\underline{\underline{\beta}}_p(t)$ describes the frictional coupling of the last shell to the remaining heat bath.

While formally equation (43) is no easier to solve than equation (42) since we must still evaluate $\underline{\underline{\beta}}_p(t)$, we can approximate $\underline{\underline{\beta}}_p(t)$ by

$$\underline{\underline{\beta}}_p(t) \cong \underline{\underline{\xi}}_p \, \delta(t) \qquad .$$

The advantage of equation (43) with the above approximation over equation (33) is the MTGLE equations include the shell structure of the solvent. One can include as many shells as necessary and only have the last shell in contact with a heat reservoir (thru the terms $\underline{\underline{\beta}}_p$ and $\underline{R}(t)$). Adelman has shown the frequencies $\underline{\underline{\omega}}^2_{e_0}$, $\underline{\underline{\omega}}^2_{e_1}$, $\underline{\underline{\Omega}}_p$, as well as $\underline{\underline{\beta}}_p$ can be calculated from molecular dynamics calculation of the solvent.[97,98]

An additional modification need be made to equation (43). First note the parameters in equation (43) are not dependent on solute configuration. Indeed, all the matrices in equation (43) are scalars for a single solute atom. For more than one solute atom, the matrices in equation (43) are non-diagonal and solute configuration-

dependent. For I_2, all the matrices become R-dependent (I-I coordinate). While there is no exact way to determine the R-dependence of $\underline{\underline{\omega}}^2_{e_0}(R)$, $\underline{\underline{\omega}}^2_{c_1}(R)$, etc., Adelman has shown that one can obtain a good approximation to these quantities with the use of linear response theory.[104,105]

The MTGLE formalism has been tested on several simple systems[92,94] where analytic results have been available. In all these cases, MTGLE has done well though these have only been one atom solute systems. For two atom solute systems comparison to analytic results is not possible, however, the frequencies determined as a function of R for several solvents[97,98] show proper qualitative behavior. Adelman has also applied the MTGLE model to I_2 recombination in $CC\ell_4$ as a solvent.[99,100] While the treatment of the electronic surfaces in that study is very crude, many important features, such as the cage effect and vibrational relaxation of I_2, agree qualitatively with the results obtained in experiment[61] and often theoretical treatment.[106]

In summary, we hope to have shown the reader how the MTGLE model differs from the Langevin model and that it does overcome the shortcomings of the Langevin model discussed in the beginning of this section. While it is clear that, computationally, equation (43) is much more difficult to implement than equation (33) (not to mention the additional work needed to evaluate the frequency parameters for each solvent), it should be equally clear that equation (43) contains many crucial dynamical effects which are absent in equation (33).

Electronic Surfaces and Electronic Transitions.

We next describe the electronic surfaces used and the model we used for the electronic transitions. In the previous section, we said recombination occured when the I-I separation < 4 Å. Because of this condition, we were able to model the electronic surfaces using only quadrupole-quadrupole interaction. While we may still use the same potential functions for large r, we must also characterize these surfaces for small r (i.e., r ∿ 2-3 Å).

In addition to the previous 10 electronic surfaces, we must also include the B state in our present calculation. We also have two of previous ten states, $A(^3\pi_{1\mu})$ and $A'(^3\pi_{2\mu})$, are substantially bound, i.e., well depth > 1000 cm^{-1}. (Several workers[65,109] have studied I_2 recombination by exciting I_2 to the A state instead of the B state). The radiative lifetime of A and A' state to the ground state is 250 μs and 6.3 ms, respectively.[110] We therefore expect, that on a picosecond timescale, some I_2 molecules recombine on the A and A' states only to radiatively decay to the ground state much later. This is, in fact, what has been observed for I_2 recombination in solid matrices by Flynn.[110] We thus have a total of four bound states, X, A', A, and B states. All these states are well-characterized and have been fitted to Morse potentials. The paramters are given in Table II. The 1 U ($^1\pi$) state has been determined by Tellinghuisen[114] to be of the form

$$V(r) = C/r^9$$

with

$$C = 7.339 \cdot 10^4 \text{ a.}\mu.$$

The additional 6 states, $^3\Pi_{0-\mu}$, $^3\Sigma^-_{(0^+)}$, $^3\Delta_{3\mu}$, $^3\Sigma^+_{\mu(0^-)}$, $^3\Pi_{2g}$, $^3\Pi_{1g}$ are all repulsive,[77] and have not been determined for small r. The only available information for these states is the estimated vertical energy determined by Mulliken.[77] We therefore arbitrarily fit these curves to the functional form:

$$V(r) = C/r^9 \tag{44}$$

determining C such that we reproduce the vertical energy. These parameters are listed in Table III. Though our characterization of these states for small r is quite arbitrary, they will not effect our results, as will be seen below.

Having characterized all the states for small r, we now join them to the quadrupole-quadrupole term to form the complete potential functions

$$r < X_m : \quad V(r) = V_<(r)$$

$$X_m \le r \le X_Q : \quad V(r) = \left[\frac{X_Q - r}{X_Q - X_m}\right] V_<(r) + \left[\frac{r - X_m}{X_Q - X_m}\right] V_Q(r)$$

$$r > X_Q : \quad V(r) = V_Q(r)$$

where

$X_Q = 5\ \mathring{A}$

$X_m = 4\ \mathring{A}$

$V_<(r)$ is either the Morse curve for the bound state or the C/r^9 curve for the repulsive states. This form of the potential guarantees us that for large r, we have the correct quadrupole-quadrupole interaction while for small r we have the proper bound and repulsive curves. Note V(r) is defined such that it is continuous.

Figure 19 shows all the curves discussed. Figure 20 shows the curves for $r > 4\ \mathring{A}$. Note the difference between this figure and figure 15, the potential curves used in the previous section. In figure 20, we see two Van der Waals type wells for the $^3\pi_{0^-\mu}$ and $^3\pi_{1g}$ states. These two states do have Van der Waals between 4-5 $\mathring{A}$ as discussed by Mulliken,[77] though our wells are merely an artifact of the potential form we have used. Figure 20 also shows many curve crossings. While the location of the curve crossings are clearly incorrect, the qualitative aspect of many crossings is probably correct in this region. What is important, from our point of view, is the curves pass very close to each other, as will be seen below. We, therefore, feel figure 20 represents the potential surfaces qualitatively accurately for the purposes at hand.

We now turn to the electronic transitions. As in the previous section, we allow electronic transitions according to the Miller-George theory, equation (34). Since our potential functions take on a more complicated form than previously, the minimum of $\Delta V(t)$ no longer occurs solely at outer turning points. We, therefore, monitor

all the surfaces during the trajectories and allow transitions to occur whenever a minimum is detected in $\Delta V(t)$. Whenever this involves only one other surface, we may use the calculated probability of equation (34) without any need for renormalization. In situations where two potential curves actually cross, the Miller-George theory predicts a transition probability of unity. While non-adiabatic coupling due to collisions probably prevents an actual crossing of curves, we would still expect the probability of transition to be large due to $\Delta V << 1$ concurrent with a large coupling. We will, therefore, follow the Miller-George theory and allow a <u>definite transition</u> at these crossing points. Since there are only 6 crossing points due to the additional structure between 4 Å and 5 Å and many other transitions occur due to minima in $\Delta V(t)$, these transitions actually make up a small percentage of the total allowed.

The last electronic transition we need discuss is the $B \rightarrow 1U$ transition involved in the collisional predissociation. Unlike the above situation the crossing of the 1U (and the other repulsive states) and B state are the <u>only</u> possible transitions out of the B state so we must be careful. Studies by Tellinghuisen,[115] Chutjian,[116] and Lehmann, <u>et al.</u>[117] have shown in the gas-phase the only symmetry-allowed transition from the B state is to the 1U and A states of which only the $B \rightarrow 1U$ transition has a relatively short lifetime of ~ 1 μsec. Unfortunately, since we are in the liquid phase, collisions not only break the symmetry restrictions allowing transitions to any of the electronic states near the B state, but also increase the predissociation rate constant to ~ 0.1 psec^{-1}.[61] Since it is important we reproduce the predissociation rate correctly, we

treat this transition phenomenologically--we allow for a fixed probability of transition to the 1U state only from the B state at the crossing point such that the proper rate constant is produced. This is basically equivalent to the method used by Adelman[102] for the predissociation step. While we could allow for some of the trajectories to dissociate to the other repulsive curves, this was deemed unnecessary since all the curves mix among each other at $r > 4$ Å and would make little difference to the subsequent dynamics. This phenomenological approach to the predissociation transition does not effect our main question which is what effect electronic transitions occurring at large r have on the recombination process.

We have chosen to look at I_2 recombination in $CC\ell_4$. This solvent choice was motivated by several reasons. First, Adelman has already calculated the relevant frequencies for this system and calculated the I_2 recombination with a crude electronic transition model. In the model used by Adelman, electronic transition from the B to 1U state is similar to ours, but for the $1U \rightarrow X$ state, he uses a procedure similar to the predissociation transition. (He does not consider any other states). We on the other hand, have transitions among 10 electronic states in the region of $r > 4$ Å, and, so, can compare oure results to his to assess the effect of these transitions. Secondly, data for I_2 recombination in $CC\ell_4$ is available so we may make some comparison to experiment.

Following Adelman,[102] we consider recombination to occur if I_2 is on the ground state and its vibrational quantum number is less than 94. We start the trajectories at $r = 2.717$ Å, the inner turning point of the B state. We started 83% of the trajectories on the B

state, 17% on the 1U state to simulate the 5.18:1.00 oscillator strength. Velocities for the iodine atoms where selected from a thermalized distribution subject to the constraint that the relative velocity was zero. The initial conditions for the MTGLE model were chosen according to Adelman's prescription.[101] Due to the complex nature of equation (43), we were only able to run 60 trajectories for 20 psec of real time due to CPU limitations.

Results and Discussion

Figure 21 presents a bar graph of the I-I separation for trajectories that have already predissociated for one, two, and three picoseconds. We see in each of these graphs, the internuclear distance quickly becomes spread over a region of ~ 4 Å. This supports our earlier suspicion that the initial value of r chosen for the Langevin model in the last section should be selected from a range of values instead of just one.

We have also found after 20 psec, approximately 12% of the trajectories are bound in the A and A' states. This result is in agreement with recent studies done by Beeker, *et al.*[110] who found the A and A' states were populated in rare gas matrices. They suggest we should see a similar effect for large solvent molecules, as we do. Because trajectories are allowed to the A and A' states, less trajectories become available for recombination and reduce the recombination rate on a picosecond timescale. (These I_2 molecules will eventually radiate down to the ground state as discussed above.)

The main result of this calculation is figure 22, the recombination rate as a function of time. We see that by 20 psec,

$\sim$ 20% of the I_2 atoms have recombined. This is to be compared to the results obtained by Adelman also presented in figure 22. The difference in our results is similar to the difference we observed in the previous section between our results and those of Hynes, et al. The additional electronic surfaces "soften" the attractive ground state potential. In addition, we also have the recombination rate slowed down an additional 10% by the trajectories that become bound on the A and A' state and are no longer available to make transitions to the ground state.

It is interesting to note Eisenthal, et al.[61] measured a rate of $\sim$ 20% recombination in the first 20 psec. While this is in excellent comparison with our results, such close agreement is probably fortuitous though clearly this is both encouraging and pleasing.

IX. Iodine Recombination: Conclusion.

We have shown by using a semiclassical theory of electronic transition coupled with the Langevin model, we could correctly describe the influence of electronic surfaces on secondary recombination dynamics. We have also shown by coupling this same semiclassical theory with a Generalized Langevin model, we could describe the full iodine recombination process. In both cases the electronic surfaces were shown to slow down the recombination rate. These results show not only is it possible to describe electronic degrees of freedom within a classical framework, but one obtains meaningful results which are in qualitative agreement with experiment.

References

1. W. H. Miller, Adv. Chem. Phys. 25, 69 (1974).
2. W. H. Miller, Adv. Chem. Phys. 30, 77 (1976).
3. D. L. Bunker, Methods Comput. Phys. 10, 287 (1971).
4. R. N. Porter, L. M. Raff, Dynamics of Molecular Collisions, Part B, ed. W. H. Miller (Plenum, 1976).
5. E. E. Muschlitz, Adv. Chem. Phys. 10, 171 (1966).
6. B. A. Thrush, Ann. Rev. Phys. Chem. 19, 371 (1968).
7. F. R. Gilmore, E. Bauer, J. W. McGowan, J. Quant. Spectrosc. Radiat. Transfer 9, 157 (1969).
8. R. B. Cundall, Transfer and Storage of Energy in Molecules, eds. G. M. Burnett and A. M. North, Vol. 1, (John Wiley and Sons, Inc., 1969).
9. A. B. Callear, J. D. Lambert, Comprehensive Chemical Kinetics, eds. C. H. Bamford and C. F. H. Tipper, Vol. 3, (Elsevier Publishing Co., 1969).
10. I. W. M. Smith, The Role of the Excited State in Chemical Physics, ed. J. W. McGowan (John Wiley and Sons, Inc., 1973).
11. R. J. Donovan, D. Husain, Chem. Rev. 70, 489 (1970).
12. J. I. Steinfeld, Acc. Chem. Res. 3, 313 (1970).
13. R. F. Vasil'ev, Russ. Chem. Rev. 39, 529 (1970).
14. T. Carrington, J. C. Polanyi, MTP International Review of Science, Physical Chemistry, ed. J. C. Polanyi, Vol. 9 (University Park Press, 1972).
15. D. H. Stedman, D. W. Setzer, Prog. React. Kinet. 6, 193 (1972).
16. J. C. Tully, Dynamics of Molecular Collisions, Part B, ed. W. H. Miller (Plenum, 1976).

17. W. H. Miller, T. F. George, J. Chem. Phys. 56, 5637 (1972).

18. J. C. Tully, R. K. Preston, J. Chem. Phys. 55, 562 (1971).

19. W. H. Miller, J. Chem. Phys. 68, 4431 (1978).

20. L. D. Landau, Physik. Z. Sowjetunion, U.R.S.S., 2, 46 (1932).

21. W. H. Miller, C. W. McCurdy, J. Chem. Phys. 69, 5163 (1978).

22. C. W. McCurdy, H. D. Meyer, W. H. Miller, J. Chem. Phys. 70, 3177 (1979).

23. H. D. Meyer, W. H. Miller, J. Chem. Phys. 71, 2156 (1979).

24. H. D. Meyer, W. H. Miller, J. Chem. Phys. 72, 2272 (1980).

25. H. D. Meyer, W. H. Miller, J. Chem. Phys. 70, 3214 (1979).

26. S. C. Mehrota, J. E. Boggs, J. Chem. Phys. 63, 4618 (1975).

27. G. D. Billing, Chem. Phys. 9, 359 (1975).

28. G. D. Billing, Chem. Phys. Lett. 30, 391 (1975).

29. K. J. McCann, M. R. Flannery, Chem. Phys. Lett. 35, 124 (1975).

30. K. J. McCann, M. R. Flannery, J. Chem. Phys. 63, 4695 (1975).

31. F. L. Pilar, Elementary Quantum Chemistry, (McGraw-Hill, Inc. 1968), p. 78.

32. M. S. Child, Molecular Collision Theory, (Academic Press, 1974), p. 141.

33. J. B. Delos, W. R. Thorson, S. K. Knudson, Phys. Rev. A 6, 709 (1972).

34. E. C. G. Stückelberg, Helv. Phys. Acta 5, 369 (1932).

35. The quantum coupled-channel program was supplied by NRCC, the National Research for Chemical Computations.

36. W. H. Miller, J. Chem. Phys. 68, 4431 (1978).

37. R. N. Porter, L. M. Raff, Dynamics of Molecular Collisions, Part B, ed. W. H. Miller (Plenum, 1976).

38. R. E. Langer, Phys. Rev. 51, 669 (1937).

39. Y. A. Schreider, The Monte Carlo Method (Pergamon Press, Inc. 1966).

40. I. H. Zimmerman, T. F. George, Chem. Phys. 7, 323 (1976).

41. D. J. Nesbitt, S. R. Leone, J. Chem. Phys. 73, 6182 (1980).

42. R. J. Donovan, D. Husain, J. Chem. Soc. Faraday Trans. 62, 2987 (1966).

43. J. R. Wiesenfeld, G. L. Wolk, J. Chem. Phys. 65, 1507 (1976).

44. H. W. Lee, K. S. Lam, P. L. deVries, T. F. George, J. Chem. Phys. 73, 206 (1980).

45. D. Secrest, B. R. Johnson, J. Chem. Phys. 45, 4556 (1966).

46. A. E. Orel, D. P. Ali, W. H. Miller, Chem. Phys. Lett. 79, 137 (1981).

47. B. C. Garrett, Ph.D. thesis, University of California, Berkeley, 1977.

48. D. G. Truhlar, J. W. Duff, Chem. Phys. Lett. 36, 551 (1975).

49. M. E. Coltrin, M. L. Koszykowski, R. A. Marcus, J. Chem. Phys. 73, 3643 (1980).

50. F. Rebentrost, W. A. Lester, Jr., J. Chem. Phys. 63, 3737 (1975).

51. F. Rebentrost, W. A. Lester, Jr., J. Chem. Phys. 64, 3879 (1976).

52. F. Rebentrost, W. A. Lester, Jr., J. Chem. Phys. 67, 3367 (1977).

53. G. Baym, Lectures on Quantum Mechanics (Benjamin Cummings Publishing Company, Inc. 1969), p. 336.

54. J. C. Tully, J. Chem. Phys. 59, 5122 (1973).

55. J. C. Tully, C. A. Truesdale, J. Chem. Phys. 65, 1002 (1976).

56. See reference 37.

57. Ann E. Orel, private communication.

58. see reference 54.

59. see reference 41.

60. R. M. Noyes, Prog. React. Kin. 1, 128 (1961).

61. T. J. Chaung, G. W. Hoffman, and K. B. Eisenthal, Chem. Phys. Lett. 25, 201 (1974).

62. K. B. Eisenthal, Ultrashort Light Pulses; Picosecond Techniques and Applications, ed. S. L. Shapiro (Springer-Verlag, Berlin, 1977).

63. C. A. Langhoff, K. Gnadig, and K. B. Eisenthal, Chem. Phys. 46, 117 (1980).

64. C. A. Langhoff, B. Moore, and W. Nugent, Picosecond Phenomena II, ed. R. Hochstrasser.

65. D. F. Kelly and P. M. Rentzepis, Chem. Phys. Lett. 85, 85 (1982).

66. J. K. K. Ip and G. Burns, J. Chem. Phys. 56, 3155 (1972).

67. J. A. Blake and G. Burns, J. Chem. Phys. 54, 1380 (1971).

68. D. L. Bunker, J. Chem. Phys. 32, 1001 (1960).

69. W. H. Wong and G. Burns. J. Chem. Phys. 58, 4459 (1973).

70. D. L. Bunker and N. Davidson, J. Am. Chem. Soc. 80, 5050 (1958).

71. D. L. Bunker and B. S. Jacobson, J. Am. Chem. Soc. 94, 1843 (1972).

72. J. N. Murrell, A. J. Stace, and R. Dammel, J. Chem. Soc. Faraday Trans. II 74, 1532 (1978).

73. P. Bado, P. H. Berens, J. P. Bergsma, S. B. Wilson, K. R. Wilson, and E. J. Heller, Picosecond Phenomena III, to be published.

74. J. T. Hynes, R. Kapral, and G. M. Torrie, J. Chem. Phys. 72, 177 (1980).

75. B. Martire and R. Gilbert, Chem. Phys. 56, 241 (1981).

76. R. M. Noyes, J. Am. Chem. Soc. 77, 2042 (1955).

77. R. S. Mulliken, J. Chem. Phys. 55, 288 (1971).

78. J. C. Tully and R. K. Preston, J. Chem. Phys. 55, 562 (1971).

79. W. H. Miller and T. F. George, J. Chem. Phys. 56, 5637 (1972).

80. J. M. Deutch and I. Oppenheim, J. Chem. Phys. 54, 3547 (1971).

81. D. McQuarrie, Statistical Mechanics, ed. S. Rice, Harper & Row, p. 540.

82. Ibid., p. 440.

83. S. Chandrasekhar, Rev. Mod. Phys. 15, 1 (1943).

84. P. Turq, F. Lantelme, and N. L. Friedman, J. Chem. Phys. 66, 3039 (1976).

85. T. Einwohner and B. J. Alder, J. Chem. Phys. 57, 505 (1972); P. K. Davis and I. Oppenheim, J. Chem. Phys. 57, 505 (1972); P. K. Davis, J. Chem. Phys. 57, 517 (1972).

86. S. H. Northrup and J. T. Hynes, J. Chem. Phys. 71, 871, 884 (1979).

87. J. Troe, Ann. Rev. Phys. Chem. 29, 223 (1978); H. Hippler, K. Luther, and J. Troe, Chem. Phys. Lett. 16, 1974 (1974); K. Luther and J. Troe, Chem. Phys. Lett. 24, 85 (1974).

88. If we write the two equations of Eq. (32) together in matrix form, ξ_1 and ξ_2 become diagonal elements of a matrix, which we designate $\underline{\underline{\xi}}$.

89. J. Tellinghuisen, J. Chem. Phys. 58, 2821 (1973).

90. J. Frank, E. Rabinowitch, Trans. Faraday Soc. 30, 120 (1934).

91. S. A. Adelman, J. Chem. Phys. 71, 4471 (1979).

92. M. Berkowitz, C. L. Brooks, S. A. Adelman, J. Chem. Phys. 72, 3889 (1980).

93. S. A. Adelman, J. Chem. Phys. 73, 3145 (1980).

94. C. L. Brooks, M. Berkowitz, S. A. Adelman, J. Chem. Phys. 73,

4353 (1980).

95. S. A. Adelman, J. Chem. Phys. 74, 4646 (1981).

96. S. A. Adelman, J. Chem. Phys. 75, 5837 (1981).

97. C. L. Brooks, S. A. Adelman, J. Chem. Phys. 76, 1007 (1982).

98. C. L. Brooks, S. A. Adelman, J. Chem. Phys. 77, 484 (1982).

99. C. L. Brooks, M. W. Balk, S. A. Adelman, J. Chem. Phys. 79, 784 (1983).

100. M. W. Balk, C. L. Brooks, S. A. Adelman, J. Chem. Phys. 79, 804 (1983).

101. J. C. Dutoit, J. M. Zellweger, H. van den Bergh, J. Chem. Phys. 78, 1825 (1983).

102. Selected papers on Noise and Stochastic Processes, ed. N. Wax (Dover Publications, Inc., 1954).

103. J. Doll, J. Chem. Phys. 61, 4242 (1972).

104. H. Mori, Prog. Theor. Phys. 33, 423 (1965).

105. R. Kubo, J. Phys. Soc. Jpn. 12, 570 (1957).

106. P. J. Nesbitt, J. T. Hynes, J. Chem. Phys. 77, 2130 (1982).

107. S. A. Adelman, Adv. Chem. Phys. __, 143 ( ).

108. S. A. Adelman, Adv. Chem. Phys., in press.

109. P. Bado, P. H. Berens, K. R. Wilson, Picosecond Lasers/ Applications, ed. L. S. Goldberg, Proc. Photo-Optic Instrum. Engin. 230, p. 322 (1982).

110. P. Beeker, E. A. Hanson, G. W. Flynn, J. Chem. Phys. 78, 5892 (1983).

111. J. Tellinghuisen, Chem. Phys. Lett. 49, 485 (1977).

112. G. E. Hall, W. J. Marinelli, P. L. Houston, J. Chem. Phys. (submitted).

113. A. J. Stace, J. N. Murrel, Mol. Phys. 33, 1 (1977).

114. J. Tellinghuisen, J. Chem. Phys. 58, 2821 (1973).

115. J. Tellinghuisen, J. Chem. Phys. 57, 2397 (1972).

116. A. Chutjian, J. Chem. Phys. 51, 5415 (1969).

117. J. Vigue, M. Broyer, J. C. Lehmann, J. Chem. Phys. 62, 4941 (1975).

118. $n \equiv n_1 = 1 - n_2$.

TABLES

Table I. Potential Parameters[a]

Electronic State	C_i[b]	Degeneracy
$^1\Sigma_g^+$	0.00	1
$^3\Pi_2$	-28.99	2
$^3\Pi_{1g}$	-16.58	2
$^3\Pi_{1\mu}$	- 8.35	2
$^3\Pi_{0^-\mu}$	- 8.35	1
$^3\Pi_2$	4.17	2
$^1\Pi_\mu$	12.41	2
$^3\Delta_3$	12.41	2
$^3\Sigma_g^-$	24.82	1
$^3\Sigma_\mu^+$	33.16	1

[a]See Eq. (41).

[b]Units are hartree·bohr^5.

Table II. Morse Parameters for Bound States[a]

	A[b]	A'[c]	B[d]
D_e	$8.116 \cdot 10^{-3}$	$1.095 \cdot 10^{-2}$	$2.00047 \cdot 10^{-2}$
β	1.125	0.9498	0.9699
r_e	5.593	5.55	5.7284

[a]All values in atomic units.

[b]See reference 111.

[c]See reference 112.

[d]See reference 113.

Table III. Potential Parameters[a]

State	EVE[b]	C[c]
$^3\Pi_{0^-\mu}$	2.4	$6.1\cdot10^4$
$^3\Sigma^-_{g(0^+)}$	3.9	$1.8\cdot10^5$
$^3\Delta_{3\mu}$	4.7	$2.4\cdot10^5$
$^3\Sigma^+_{\mu(0^-)}$	4.5	$2.4\cdot10^5$
$^3\Pi_{2g}$	3.2	$1.3\cdot10^5$
$^3\Pi_{1g}$	3.4	$1.4\cdot10^5$

[a]See equation (44).

[b]Estimated vertical energy in eV's.

[c]In atomic units.

Figure Captions

1. Diabatic curves of equation (9) for $\alpha = 2.0$. Energy is plotted in atomic units (a. μ.) and distance is plotted in angstroms. Insert shows plot of diabatic coupling element.
2. $|S_{12}(E)|^2$ vs. energy (eV) plot for $\alpha = 2.0$. Solid line is the coupled-channel quantum results, circles are the classical analog model results. Error bars are ± 10%.
3. Same as Figure 2 with $\alpha = 1.0$.
4. Same as Figure 2 with $\alpha = 0.4$.
5. Histogram boxing for electronic-vibrational energy transfer for collinear H_2Br.
6. Transition probability as a function of spin-orbit splitting λ for initial translational energy $E_h = 0.01$ a.u. and V=1, n=0. Solid curve is exact quantum results (reference 44), dashed curve the result given by the classical model with the histogram approximation, and the dotted curve the results of the classical model with the moment method.
7. Same as figure 6 with $E_h = 0.035$ a.u.
8. Transition probability as a function of spin-orbit splitting λ(a. μ.) for initial translational energy $E_h = 0.01$ a.μ. and v=0, n=1, as calculated by the moment method. Solid line is non-resonant probability (v=0,n=1→v=0,n=0), dotted line is resonant probability (v=0,n=1→v=1,n=0).
9. Same as figure 8 with $E_h = 0.001$ a.u. (thermal energy range).
10. Transition probability vs. energy (a.u.) for physical value of λ as calculated by the moment method. Solid line is the

non-resonant probability, dotted line is the resonant probability.

11. Conventional histogram boxes and skewed histogram boxes for FH_2 calculations. See text for further details.

12. Geometrical averaged cross-section ($\mathring{A}^2$) vs. energy (meV) plot for FH_2 resonant reaction channel ($j = \frac{1}{2}$, N=0 $\rightarrow$ $j = \frac{3}{2}$, N=2). Solid curve is quantum results (reference 52), circles are SMM results (reference 24), crosses are the Ehrenfest model results.

13. Plot of opacity function vs. impact parameter b(a.μ.) for E_{tot} = 60 meV for FH_2 reaction. Solid curve: quantum results, dashed curve: Ehrenfest results, dotted curve: SMM results.

14. Cross section ($\mathring{A}^2$) vs. energy (eV) for BrH_2 reaction calculated using the Ehrenfest model. Crosses are the resonant channel results, circles are the non-resonant channel results.

15. Potential curves for the ten electronic states arising from two ground state ($^2P_{3/2}$) iodine atoms.

16. Probability that at time t the two iodine atoms have not recombined; T = 300^{ok}, r_o = 5.5 $\mathring{A}$. All results are from the stochastic trajectory model; curve G (the results of reference 74) utilizes the ground state I_2 potential curve for V(r) in Eq. (33), curve T utilizes the thermally averaged potential of Eq. (39) for V(r), and curve S uses the semiclassical surface-hopping model to allow V(r) to change as the electronic state of the system changes.

17. Average relative population of the 10 electronic states (state 1 is the ground state) as obtained in the stochastic surface-hopping trajectory calculation (points connected by solid lines) and as given by a Boltzmann distribution (broken curve).

(A) is for a region of large r (7-8 Å), and (B) for a region of smaller r (4-5 Å).

18. Dissociation probability, $P_\infty \equiv P(t\to\infty)$, with P(t) as shown in Figure 16 for 300°K. The labels G, T, and S have the same meaning as in Figure 16.

19. I_2 potential curves as determined by equations in the text. V(R) is in eV, R is in angstroms.

20. I_2 potentials curves for r > 4 Å and energy scale enlarged. V(R) is in eV, R is in angstroms.

21. Bar graph of I-I internuclear separation of molecules which have already predissociated: a) after one picosecond, b) after two picosecond, c) after three picosecond.

22. Probability of recombination for first twenty picoseconds; solid line, our results; dashed line, results from reference 102.

FIGURES

FIGURE 1

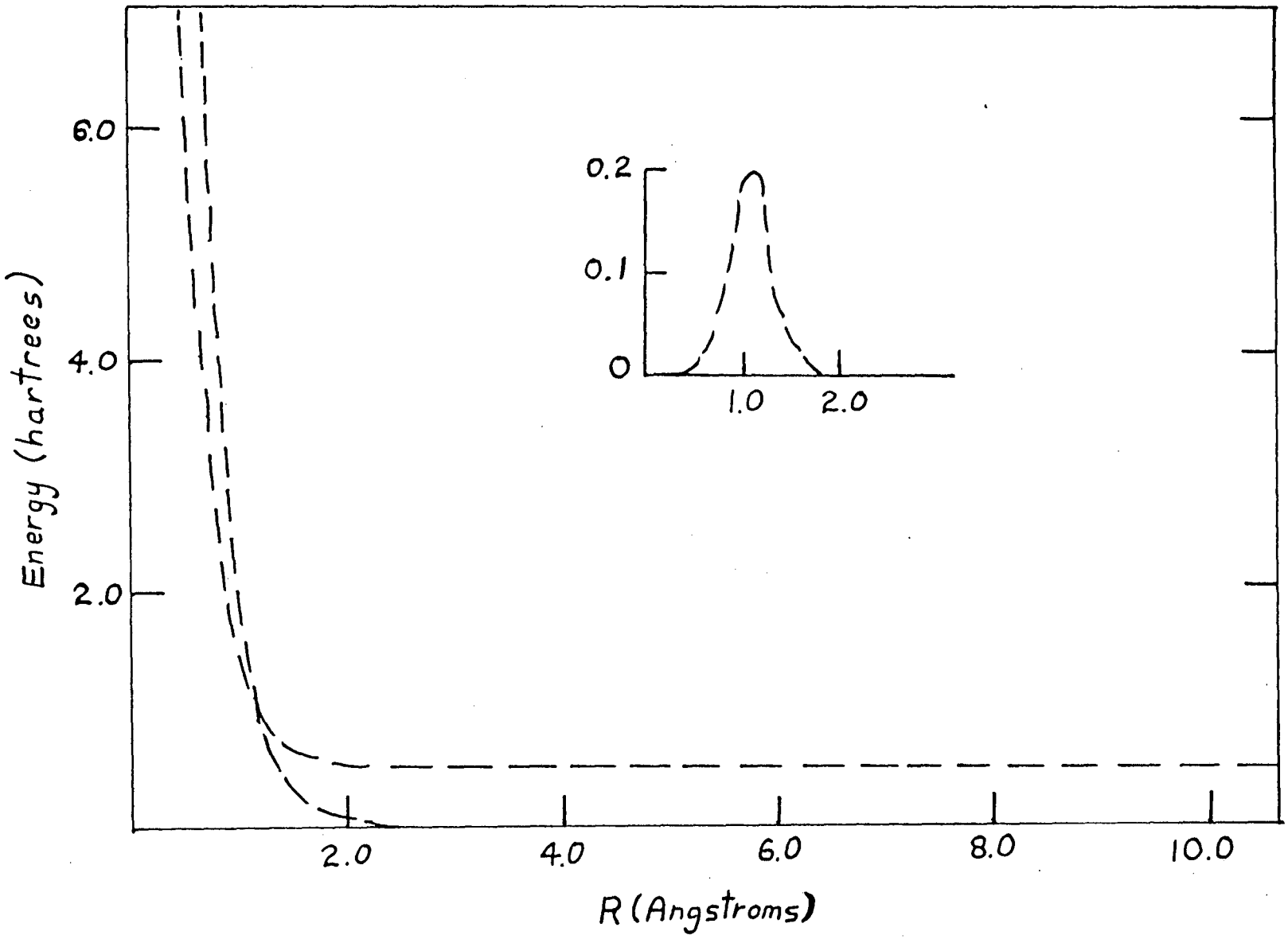
6.0
4.0
2.0
Energy (hartrees)
0.2
0.1
0
1.0
2.0
2.0
4.0
6.0
8.0
10.0
R (Angstroms)

FIGURE 2

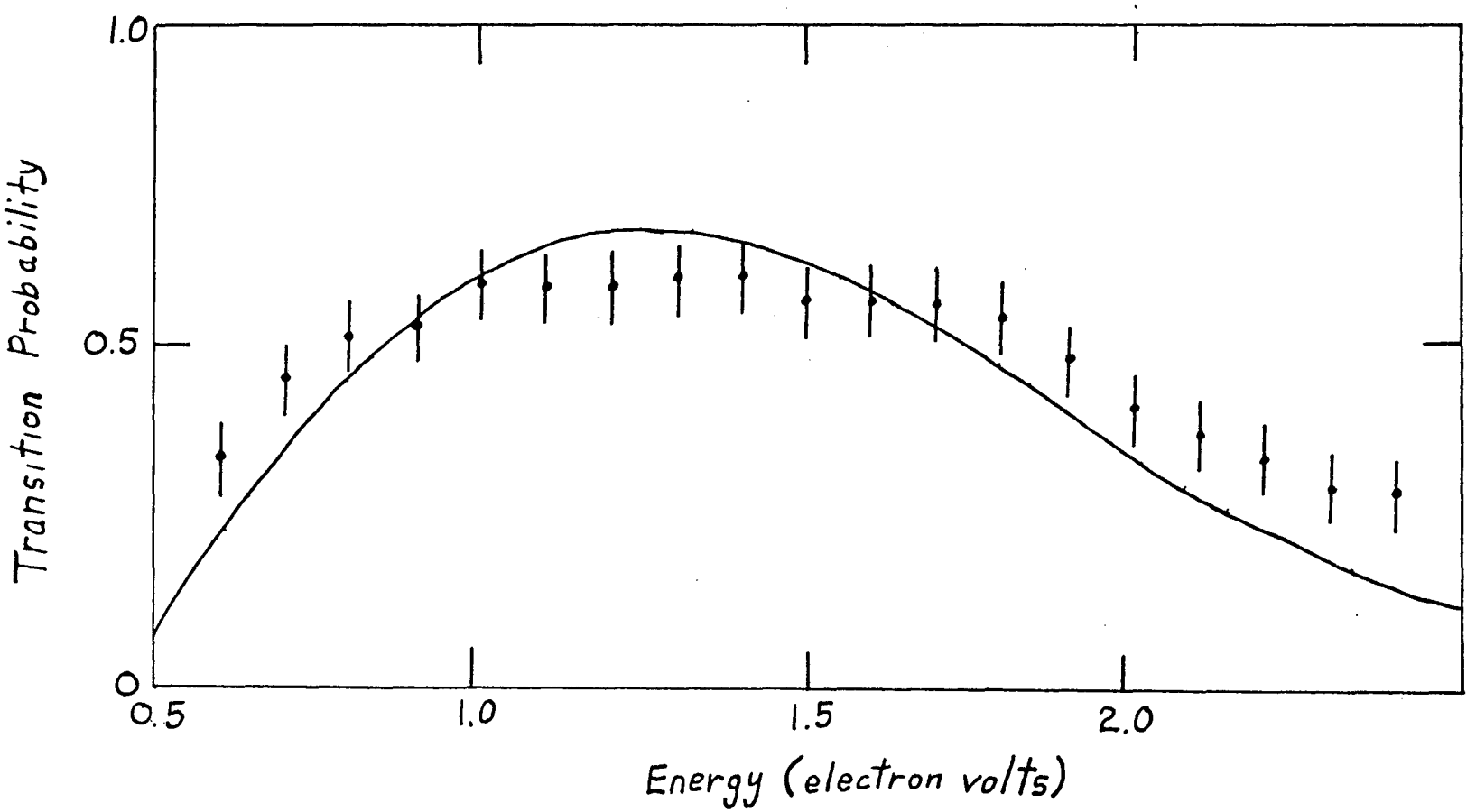
1.0
0.5
0
Transition Probability
0.5
1.0
1.5
2.0
Energy (electron volts)

FIGURE 3

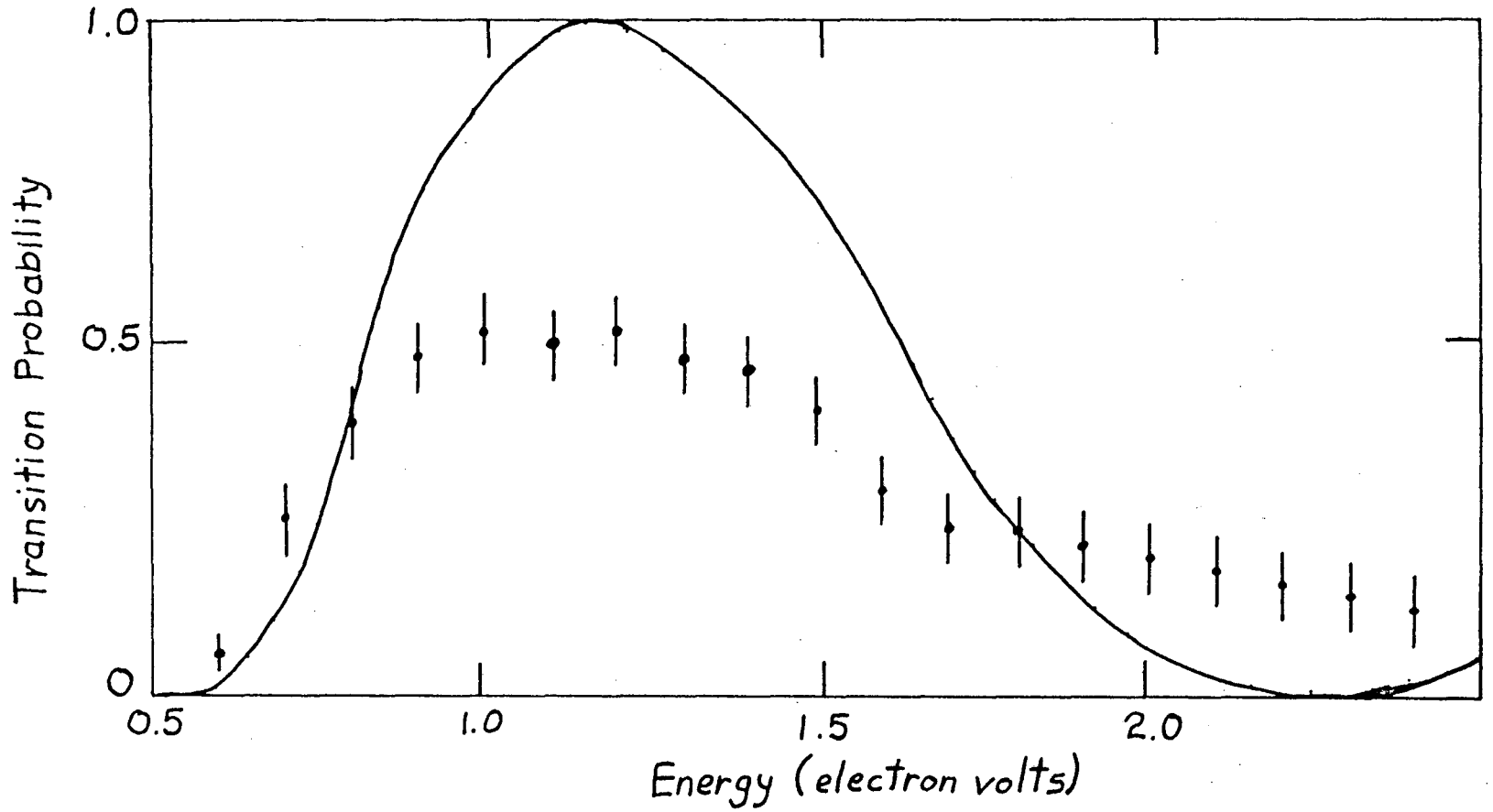
1.0
0.5
0
Transition Probability
0.5
1.0
1.5
2.0
Energy (electron volts)

FIGURE 4

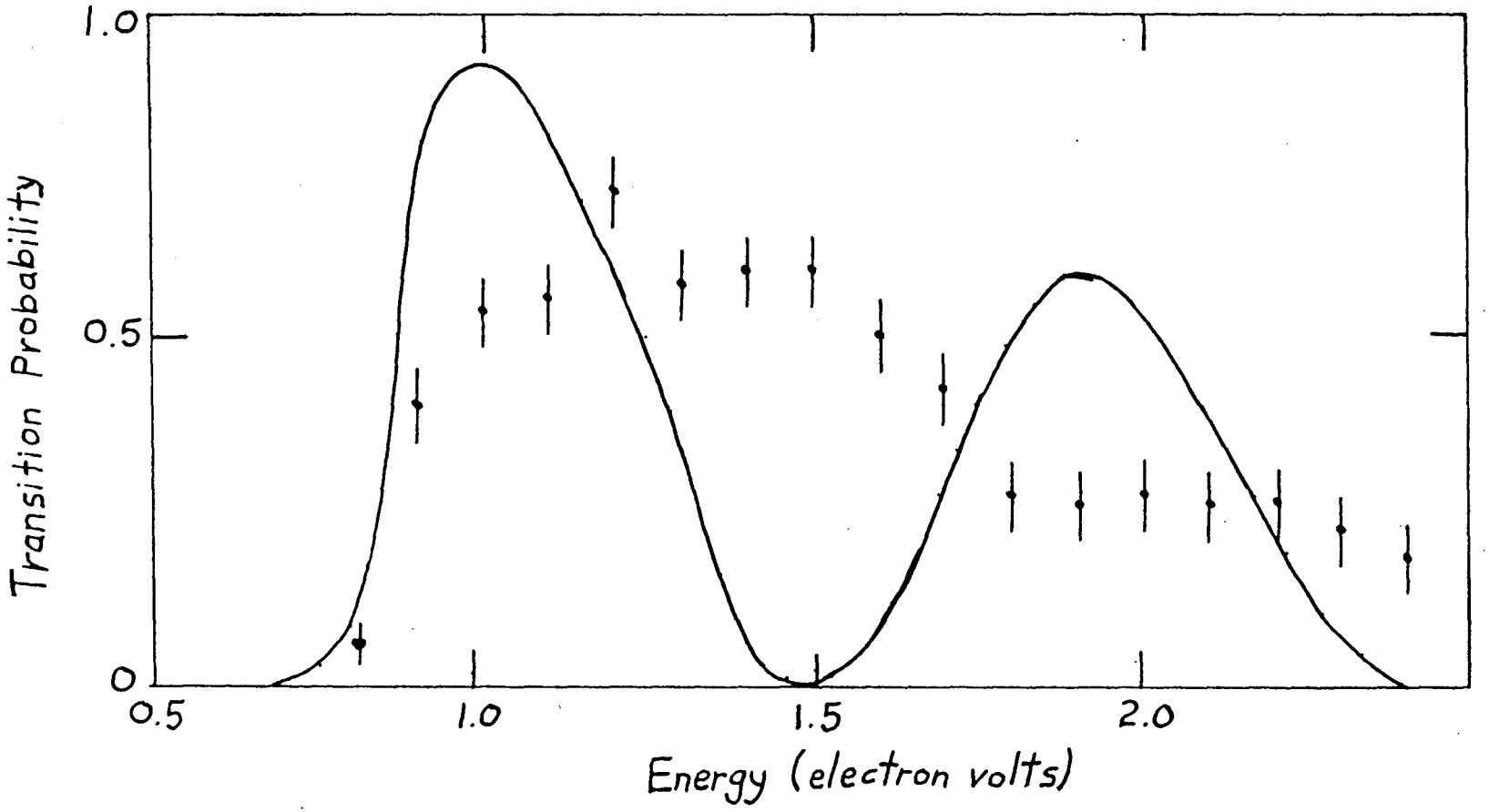
1.0
0.5
0
Transition Probability
0.5
1.0
1.5
2.0
Energy (electron volts)

N \ V	0	1
0	(0,0)	(0,1)
1	(1,0)	(1,1)

FIGURE 5

FIGURE 6

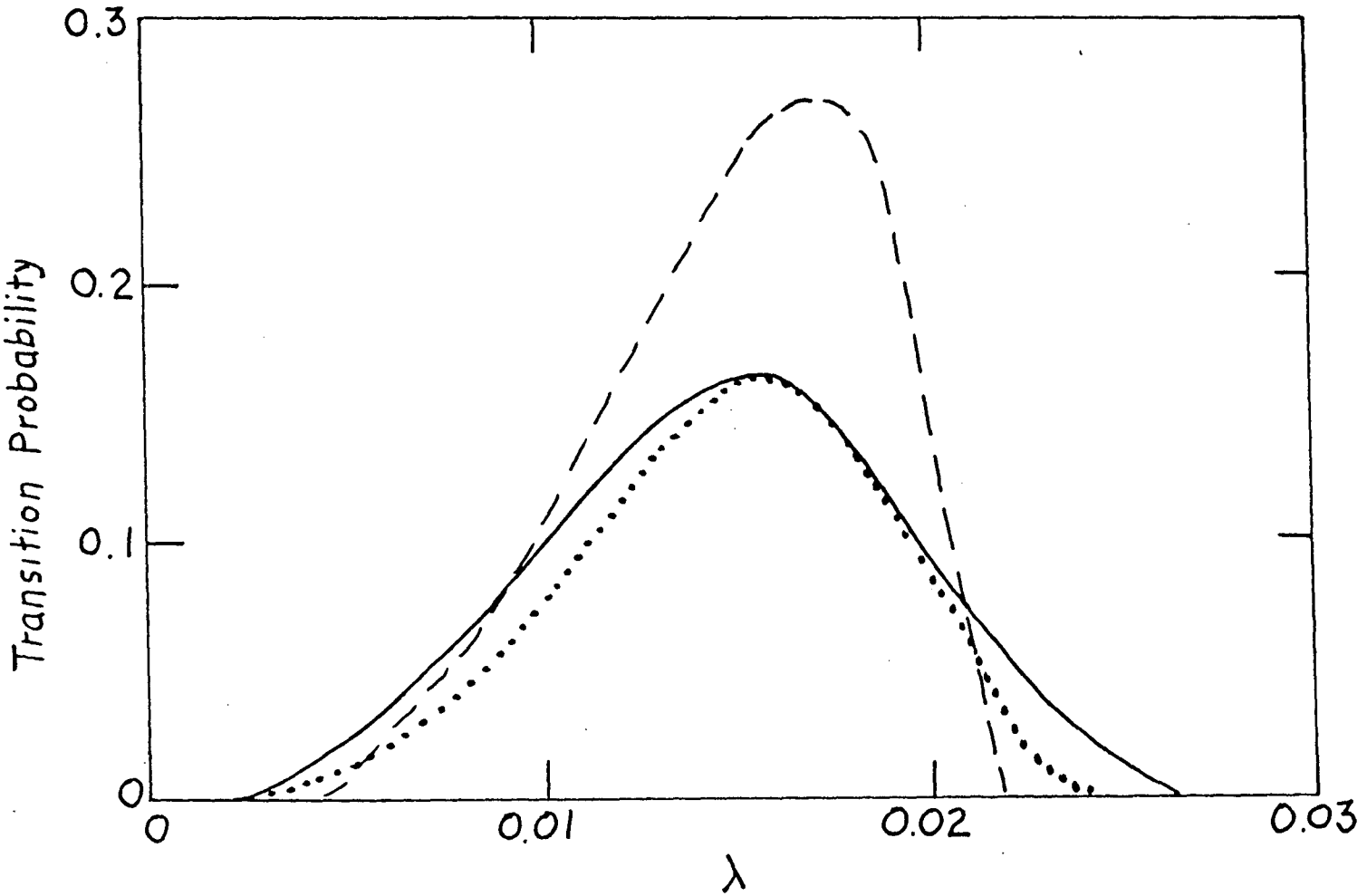

FIGURE 7

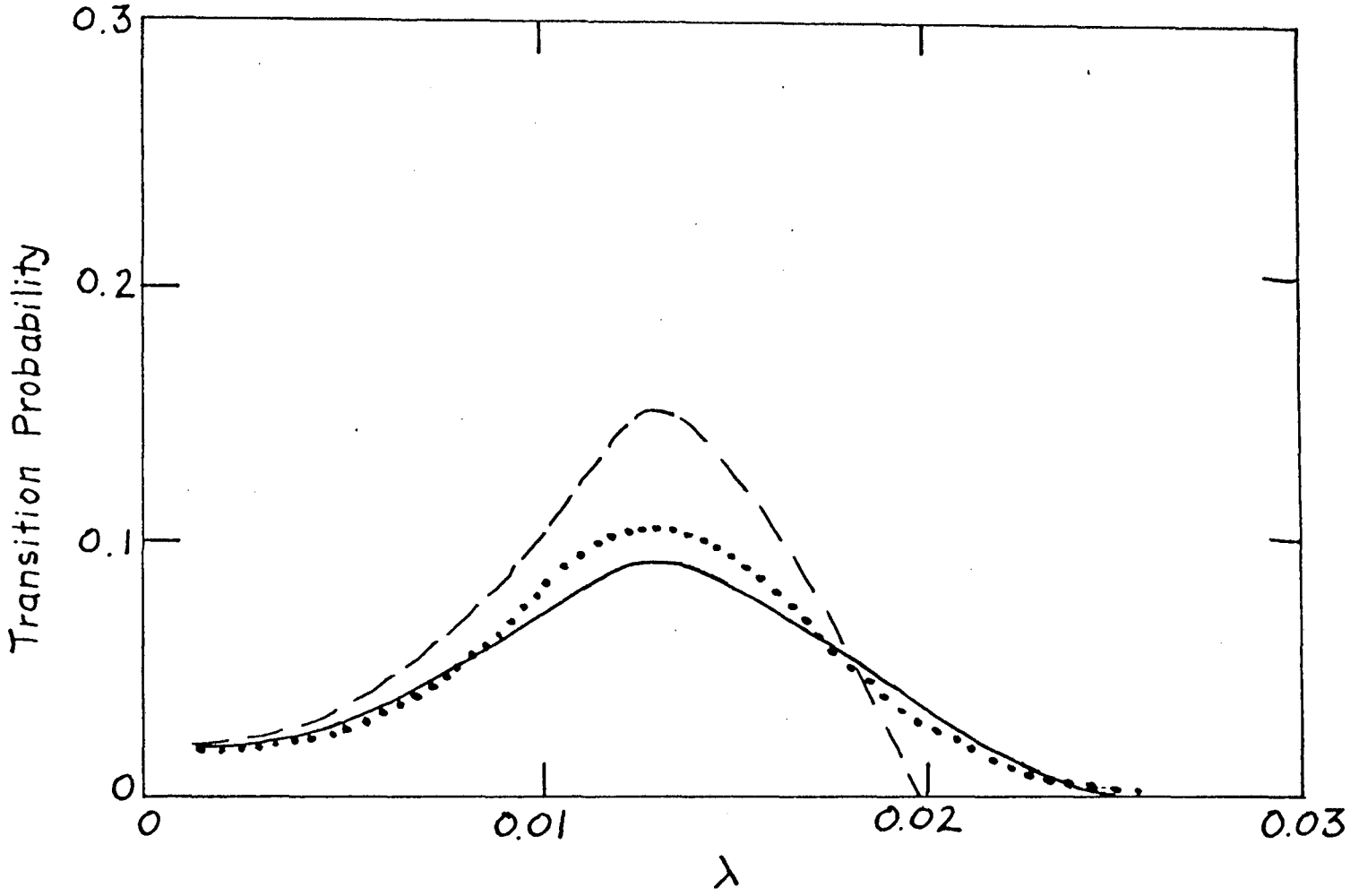

FIGURE 8

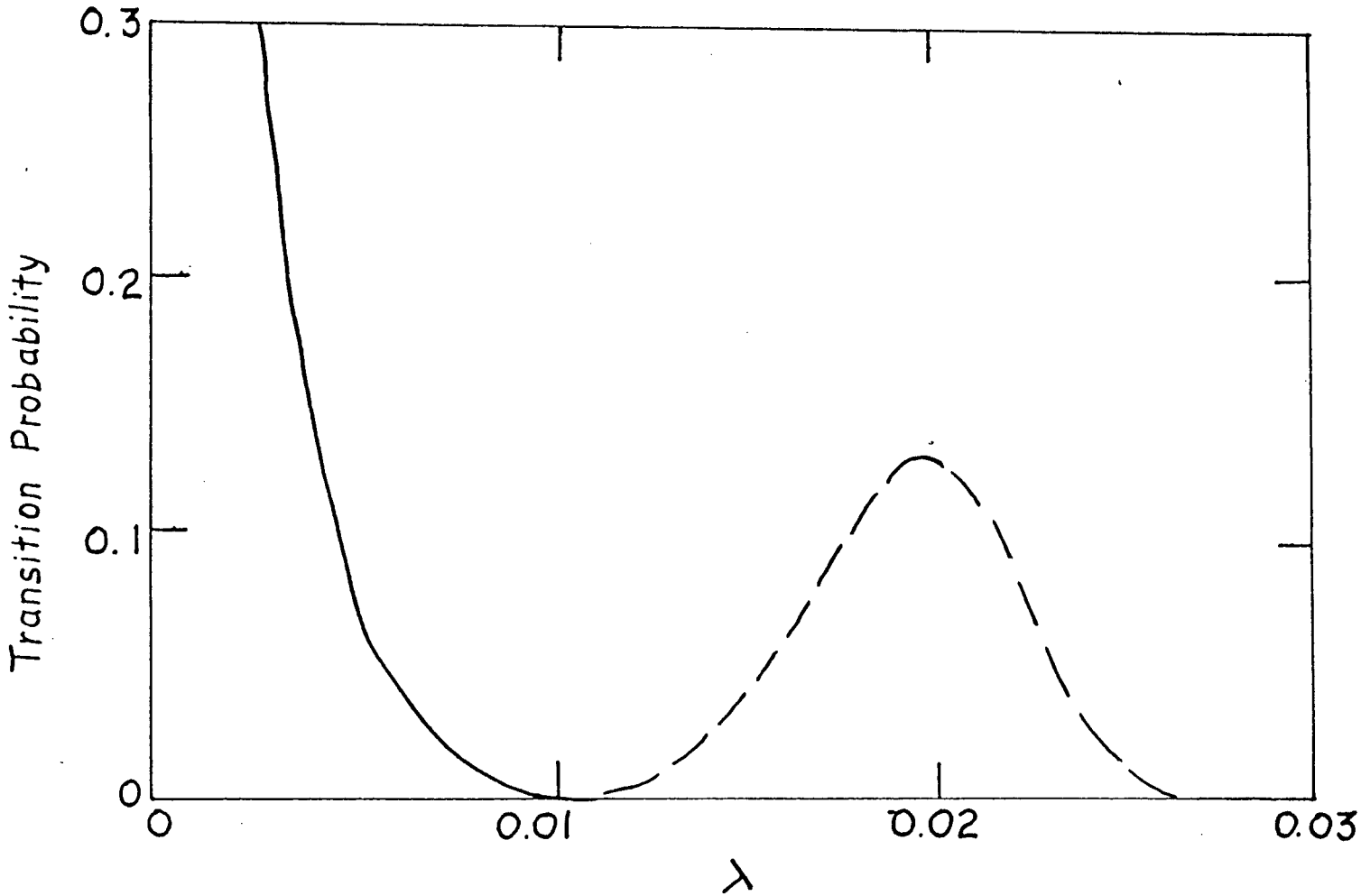

FIGURE 9

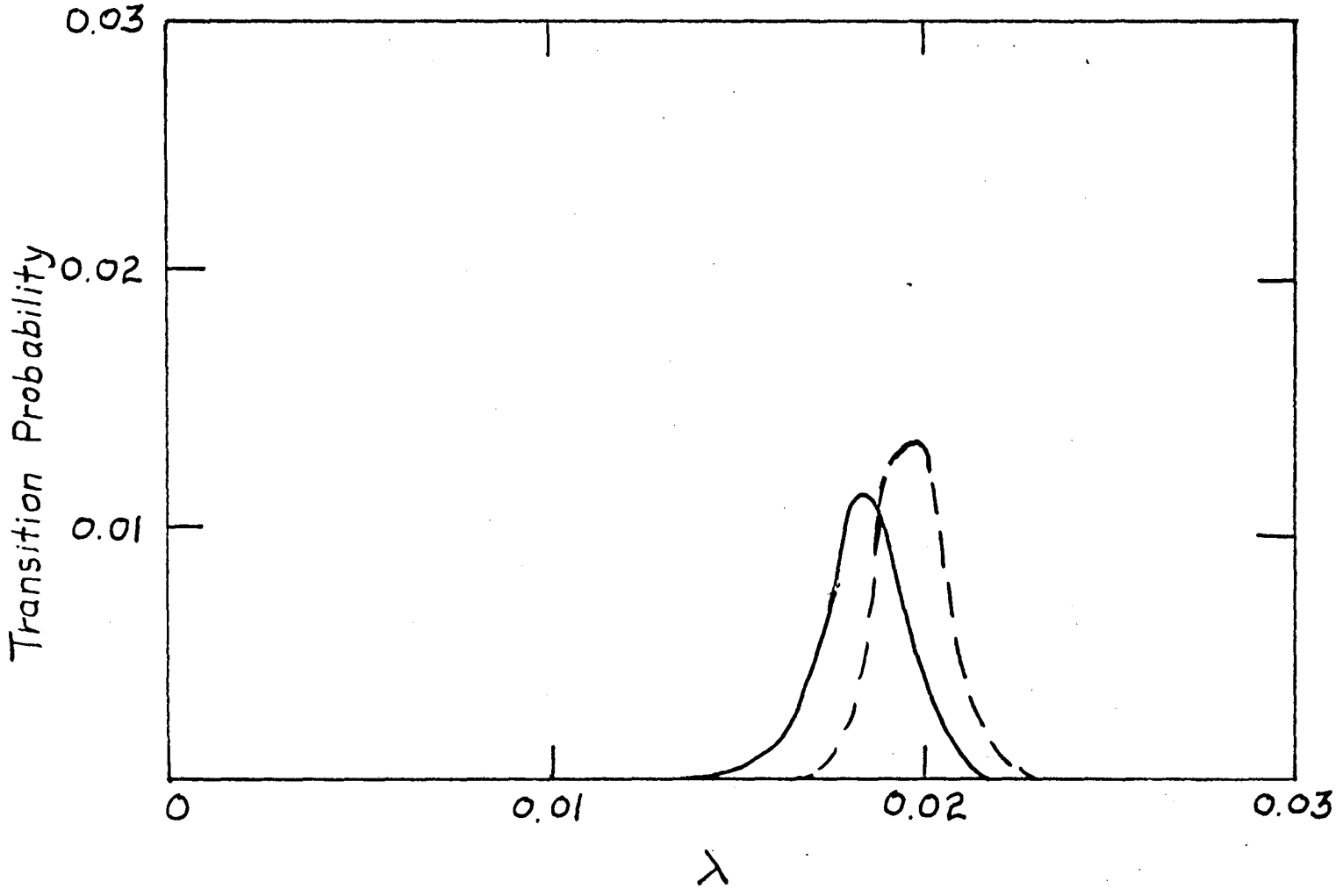

FIGURE 10

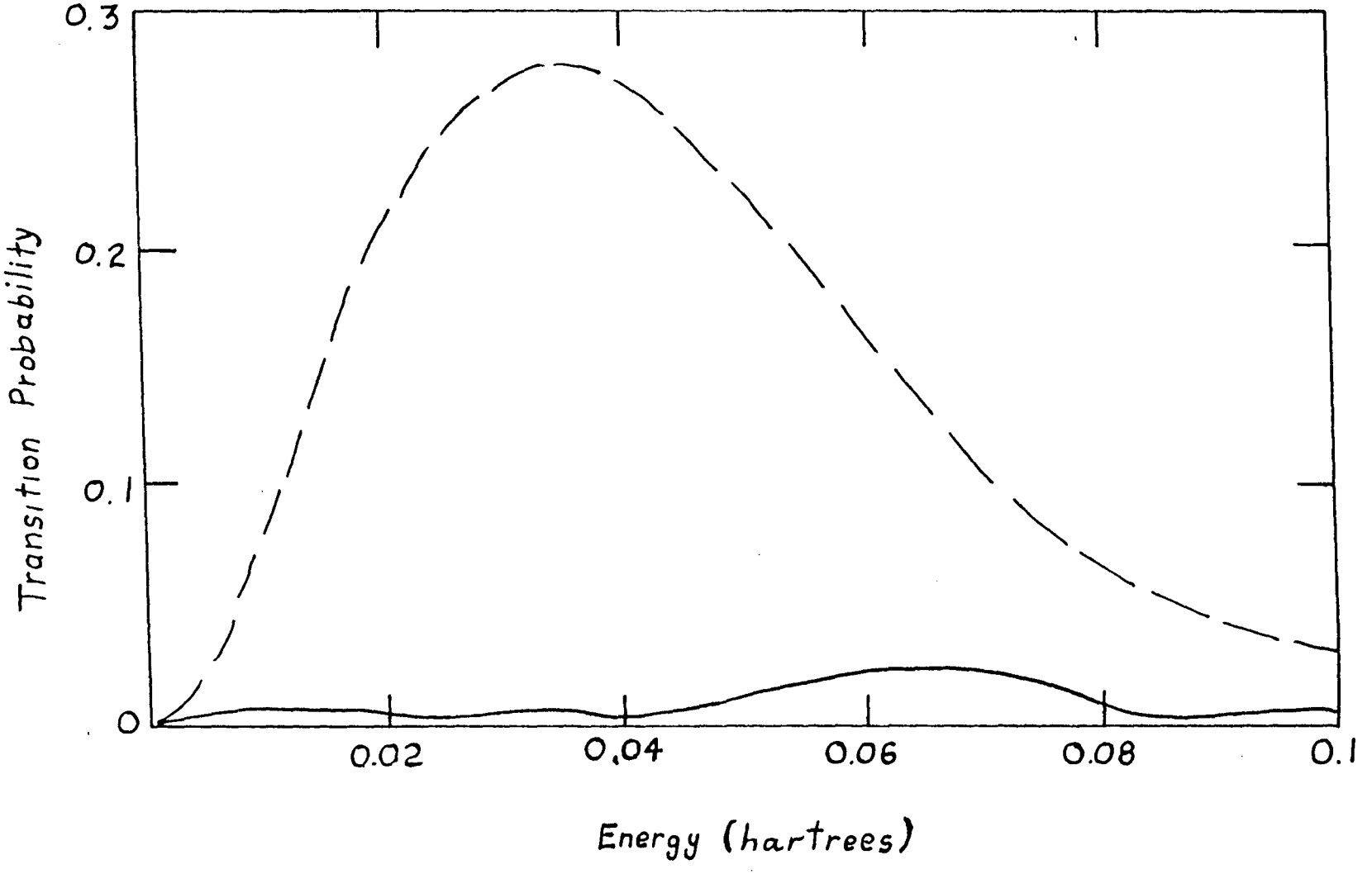
0.3
0.2
0.1
0
Transition Probability
0.02
0.04
0.06
0.08
0.1
Energy (hartrees)

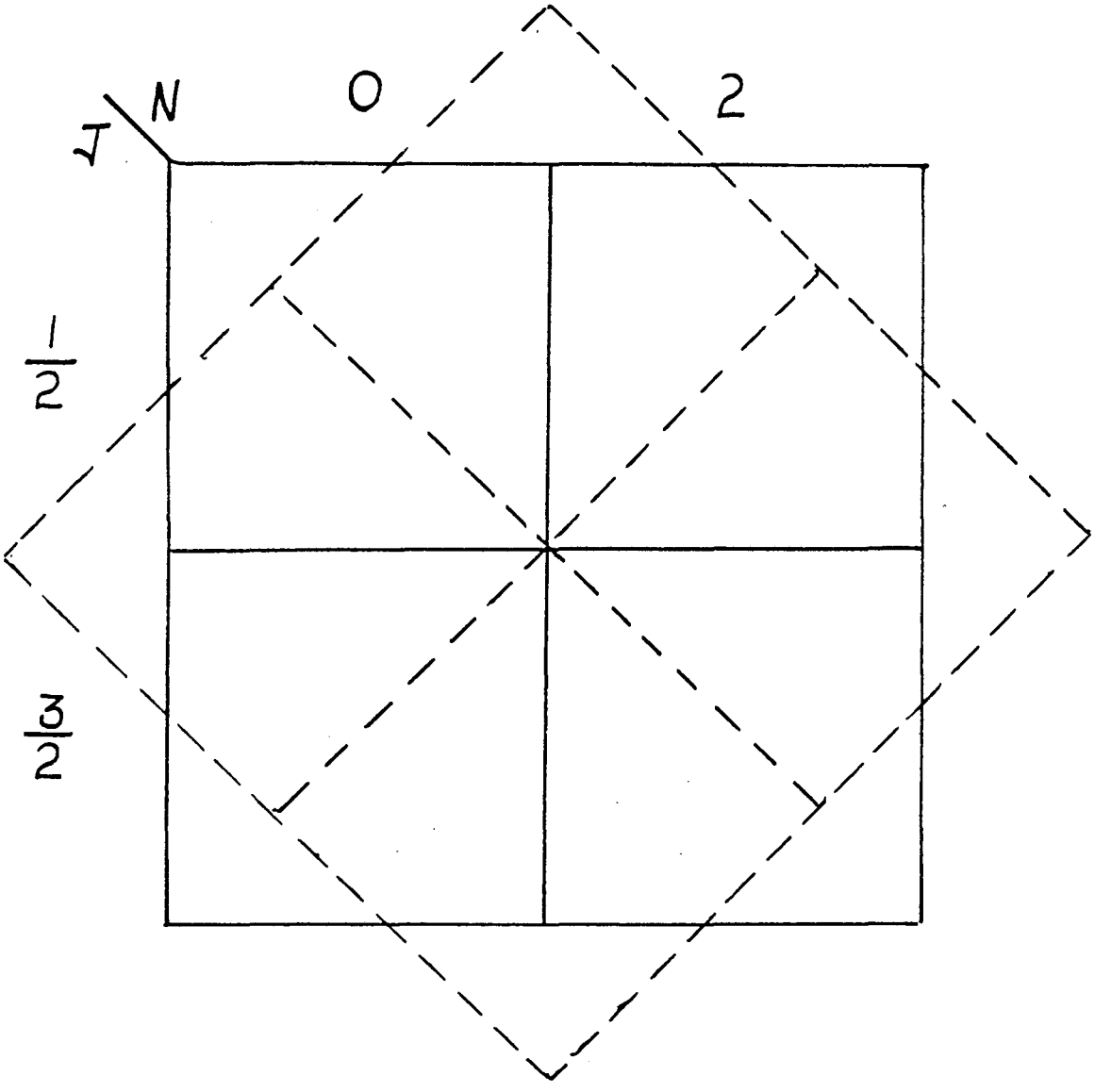

FIGURE 11

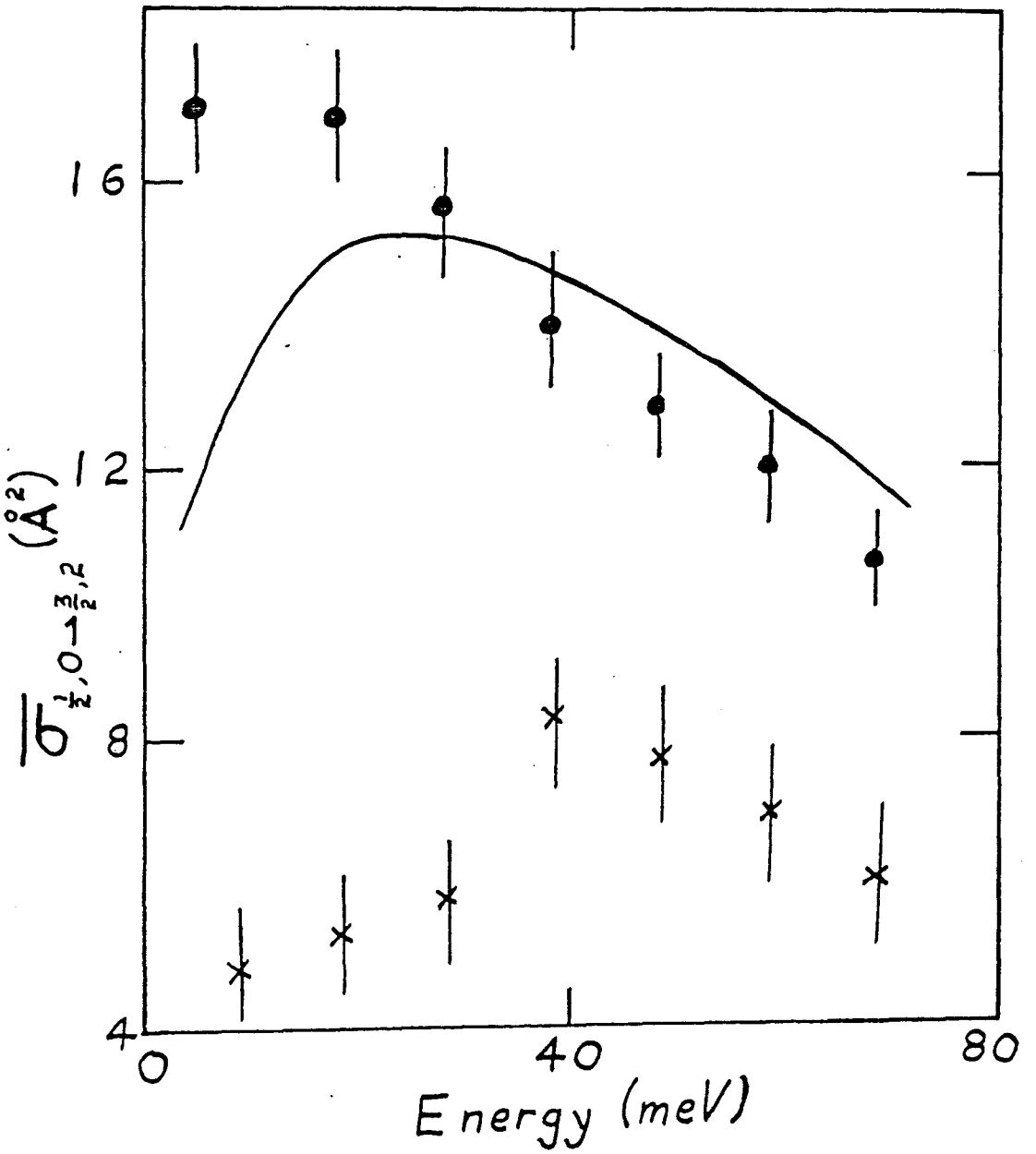
16
12
8
4
0
40
80
Energy (meV)
$\overline{\sigma}_{\frac{1}{2},0\to\frac{3}{2},2}$ (Å^2)

FIGURE 12

FIGURE 13

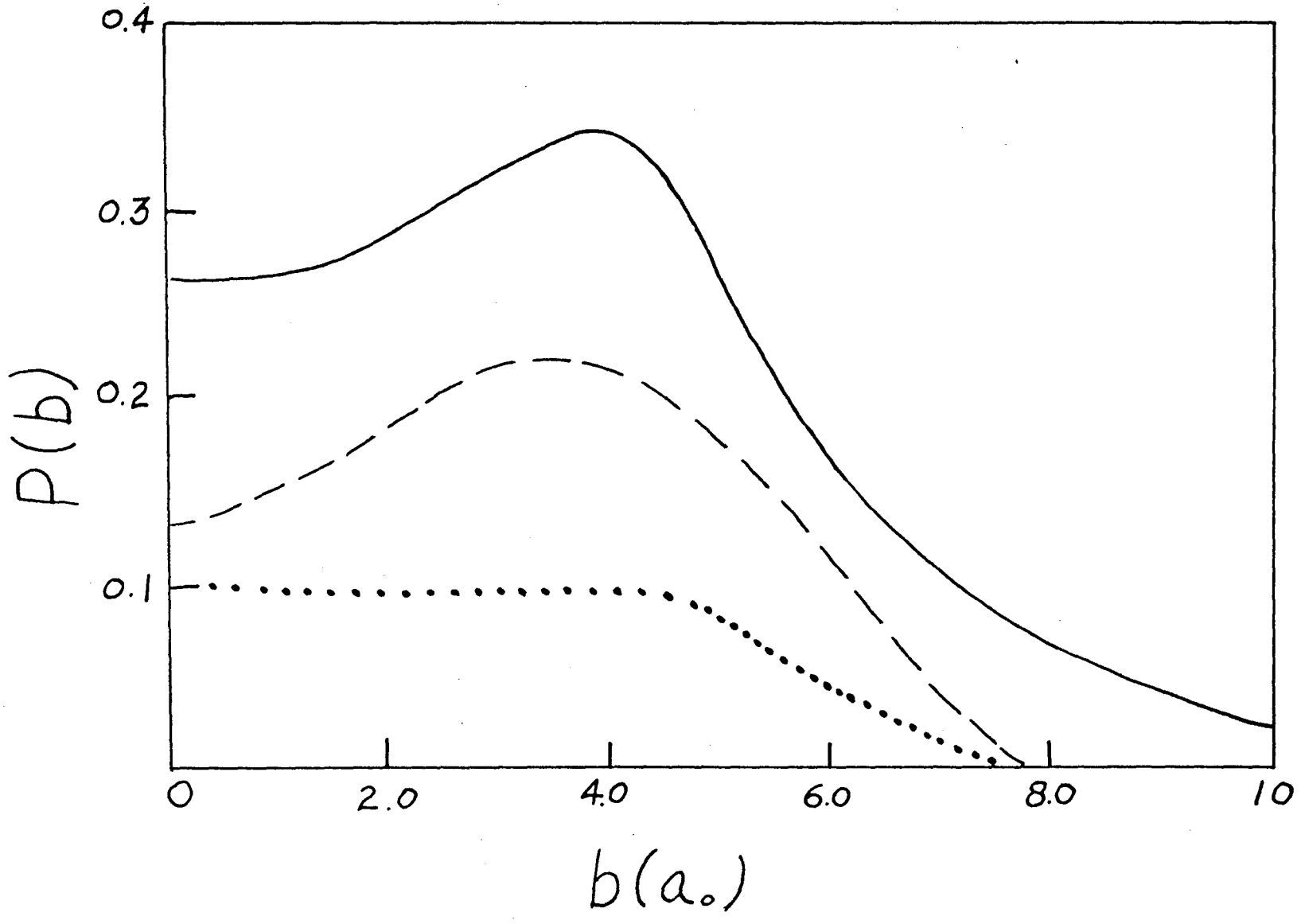

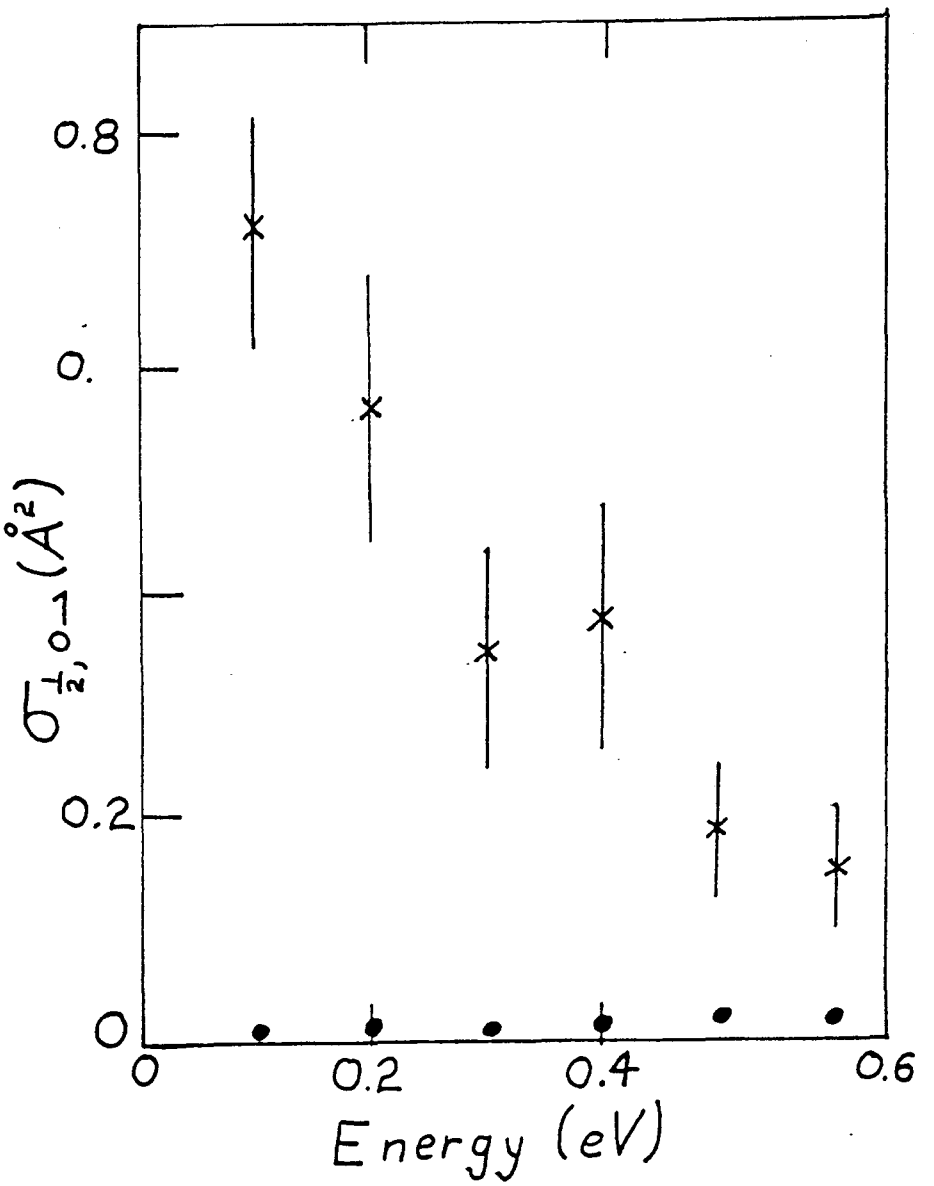

FIGURE 14

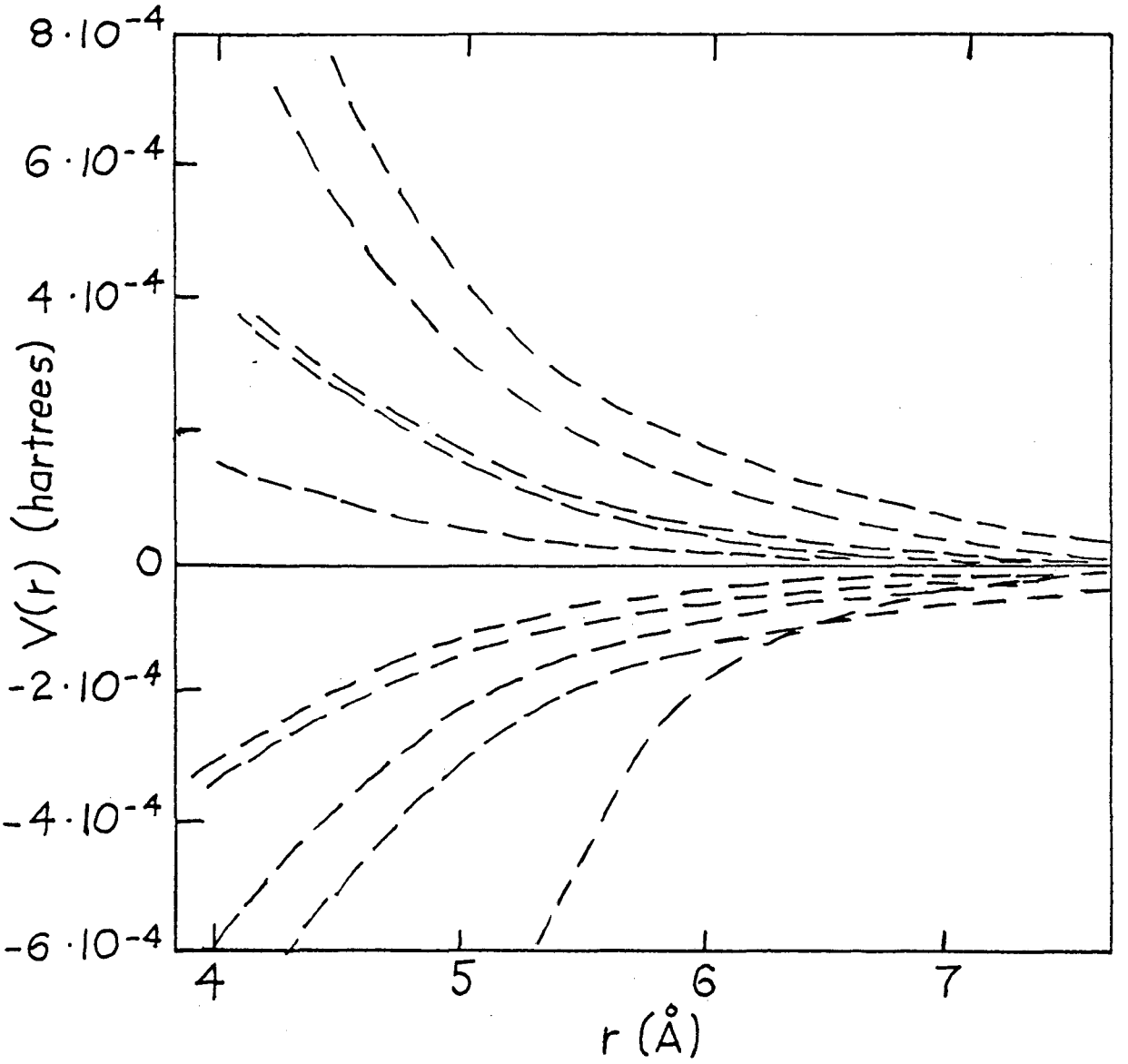

FIGURE 15

FIGURE 16

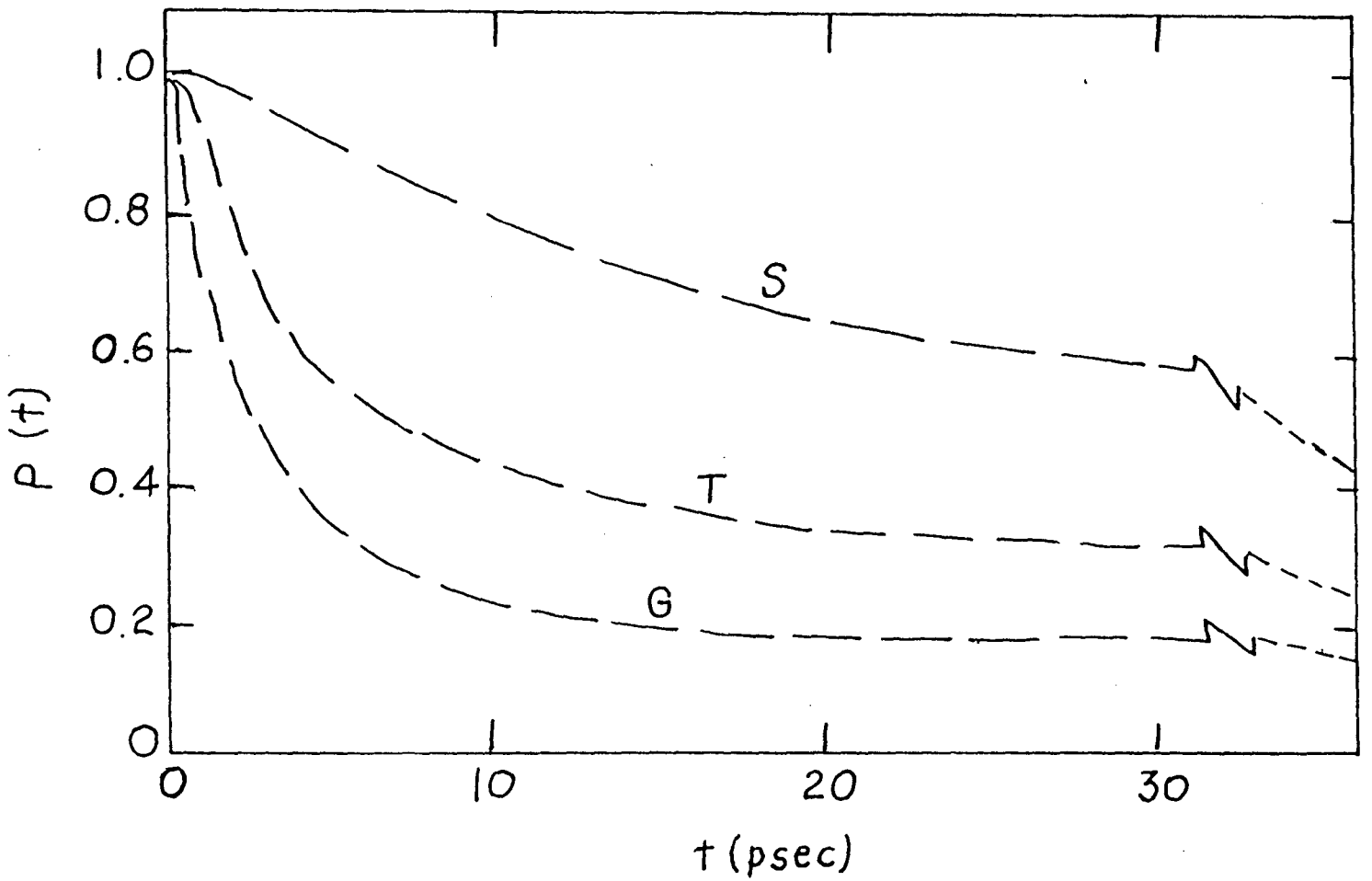

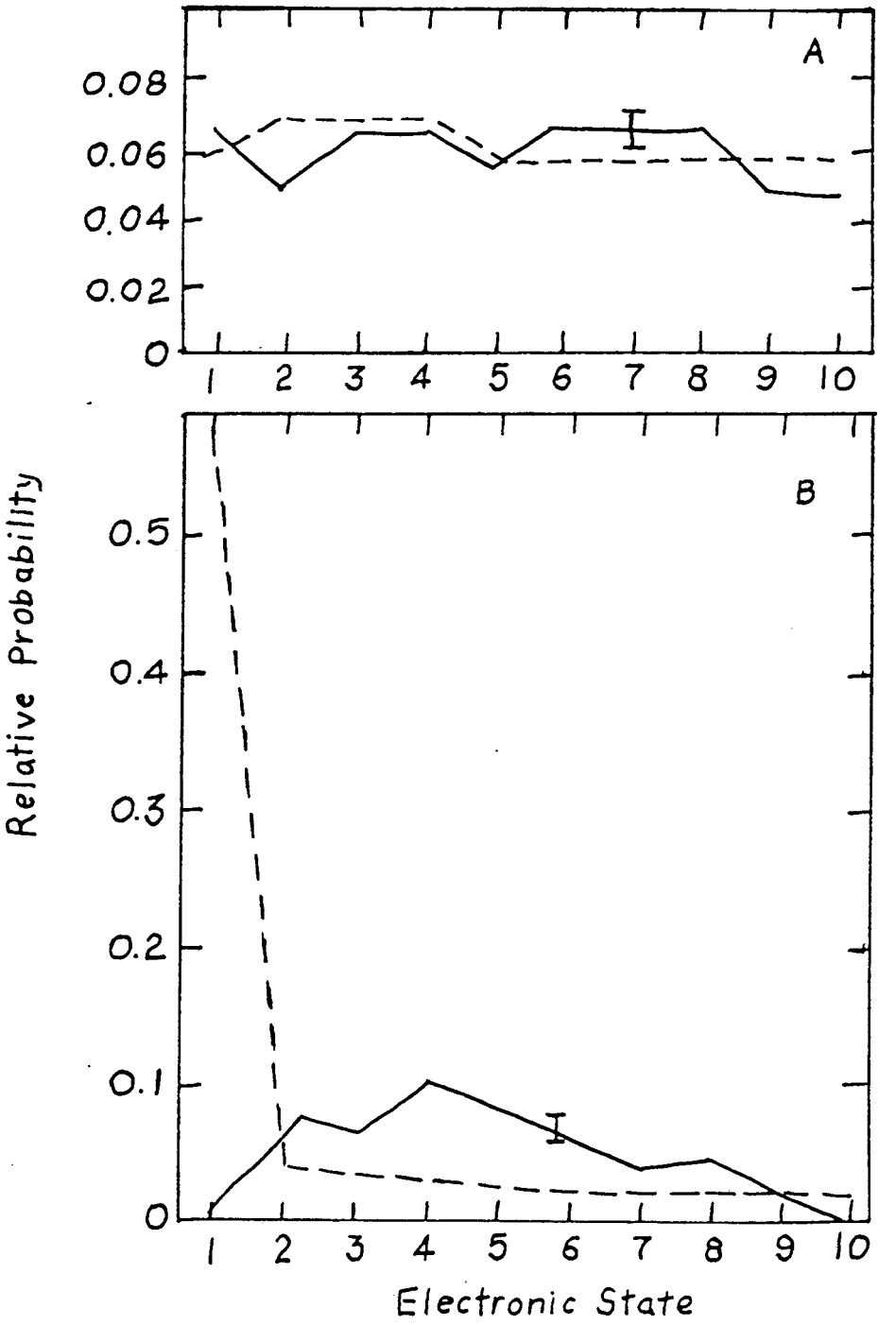
A
0.08
0.06
0.04
0.02
0
1 2 3 4 5 6 7 8 9 10
B
0.5
0.4
0.3
0.2
0.1
0
1 2 3 4 5 6 7 8 9 10
Relative Probability
Electronic State

FIGURE 17

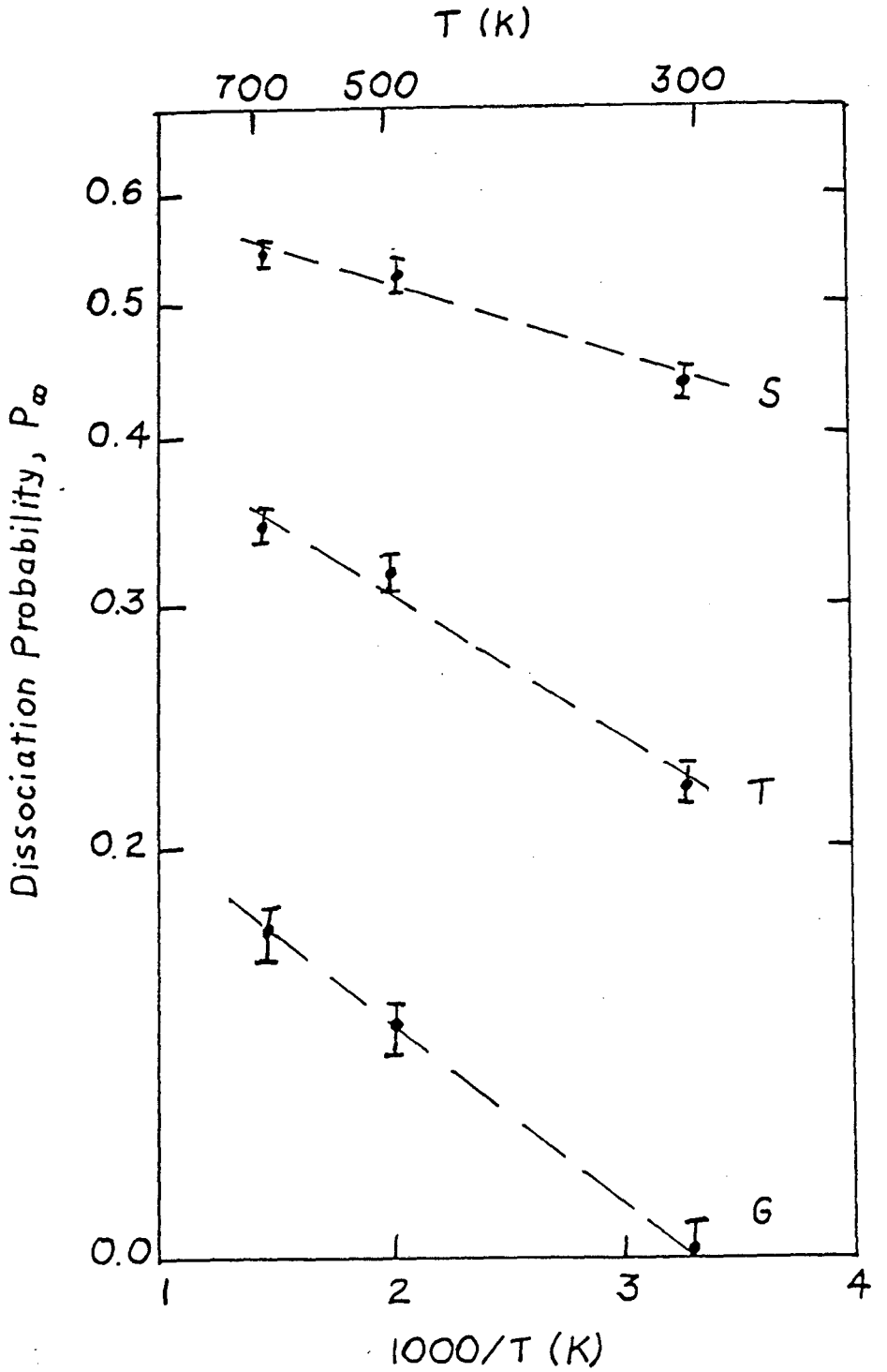
T (K)
700
500
300
0.6
0.5
0.4
0.3
0.2
0.0
Dissociation Probability, P_∞
S
T
G
1
2
3
4
1000/T (K)

FIGURE 18

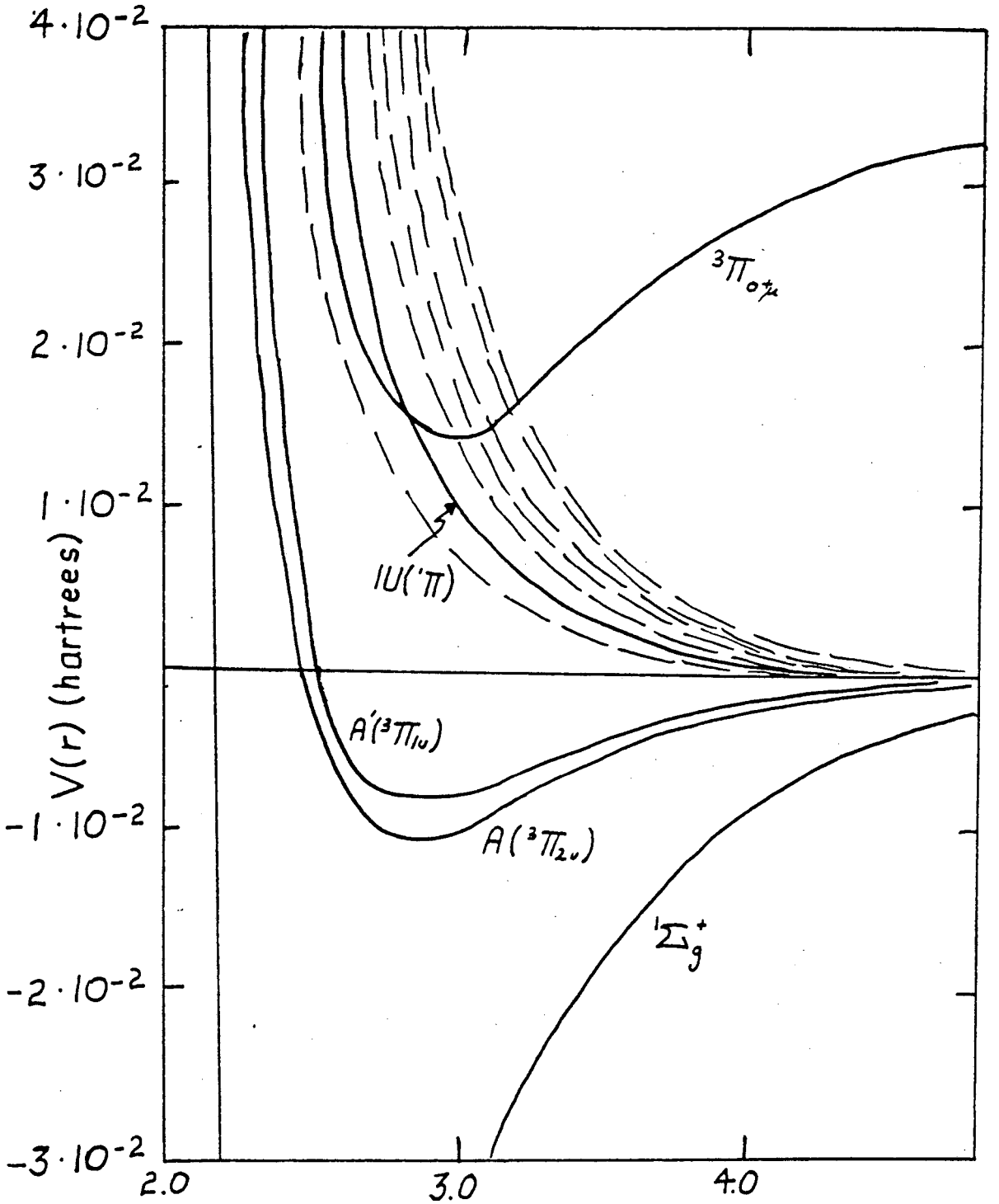
4·10⁻²
3·10⁻²
2·10⁻²
1·10⁻²
-1·10⁻²
-2·10⁻²
-3·10⁻²
V(r) (hartrees)
2.0
3.0
4.0
³Π₀₊
IU(¹Π)
A'(³Π₁ᵤ)
A(³Π₂ᵤ)
¹Σ₉⁺

FIGURE 19

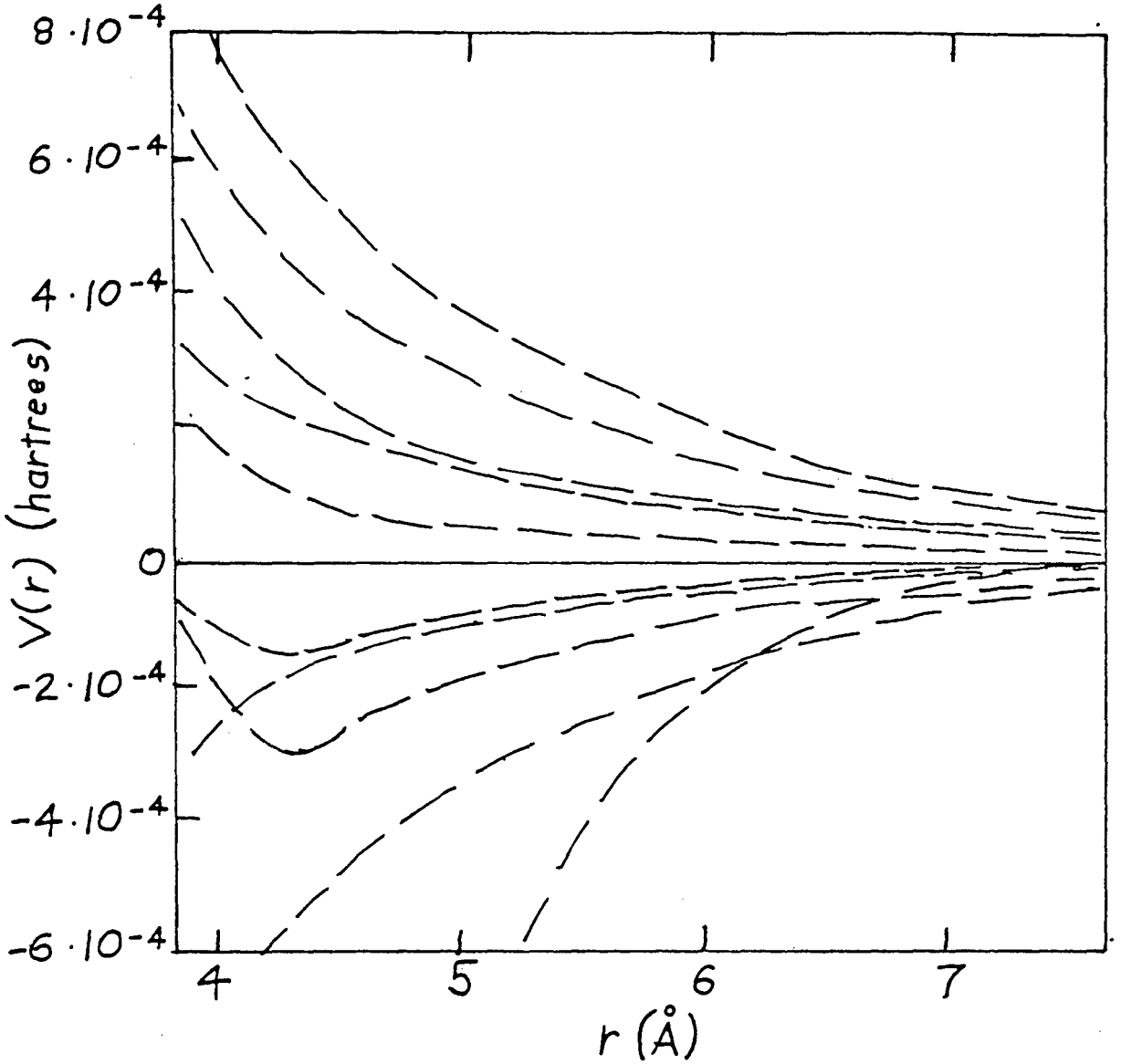

FIGURE 20

FIGURE 21

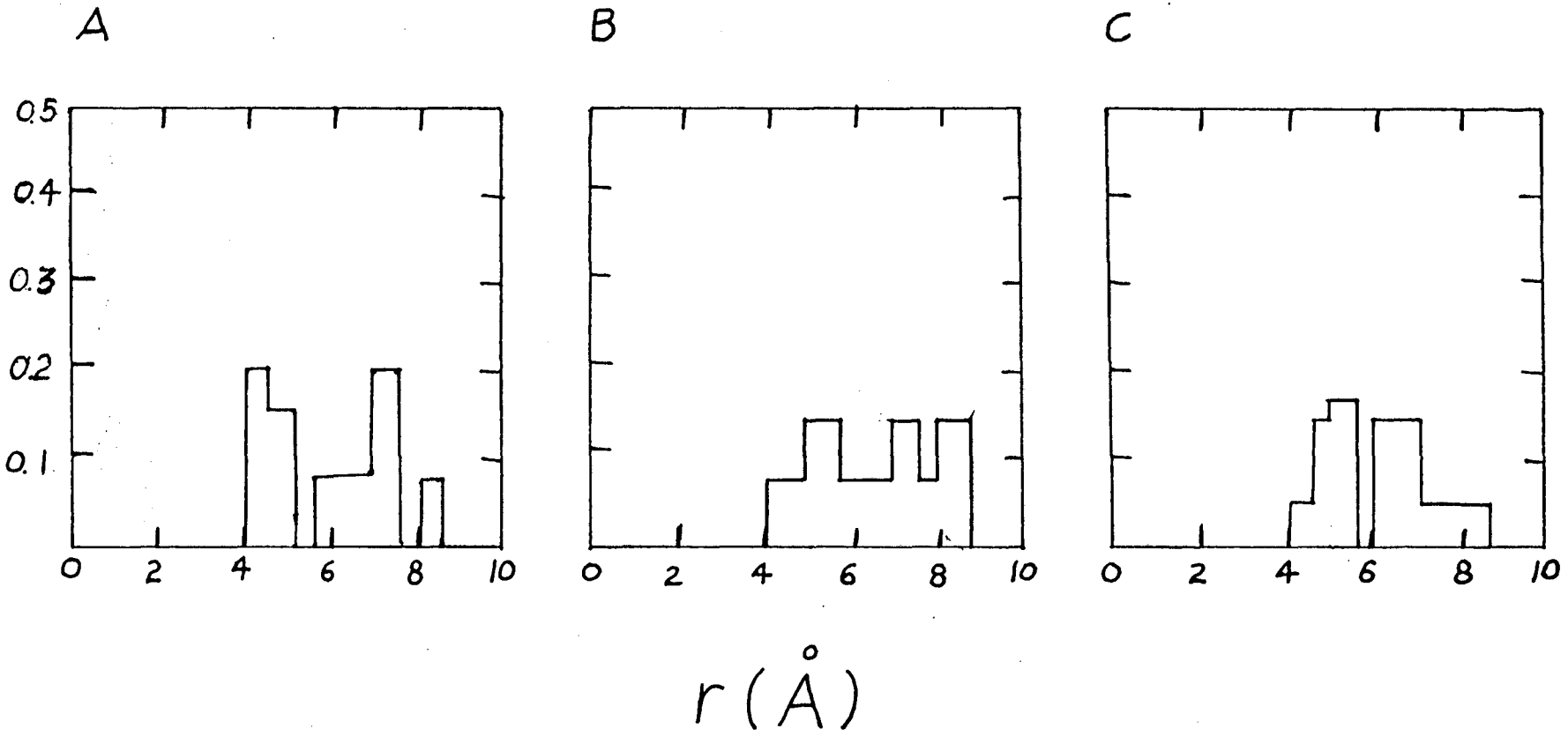

FIGURE 22

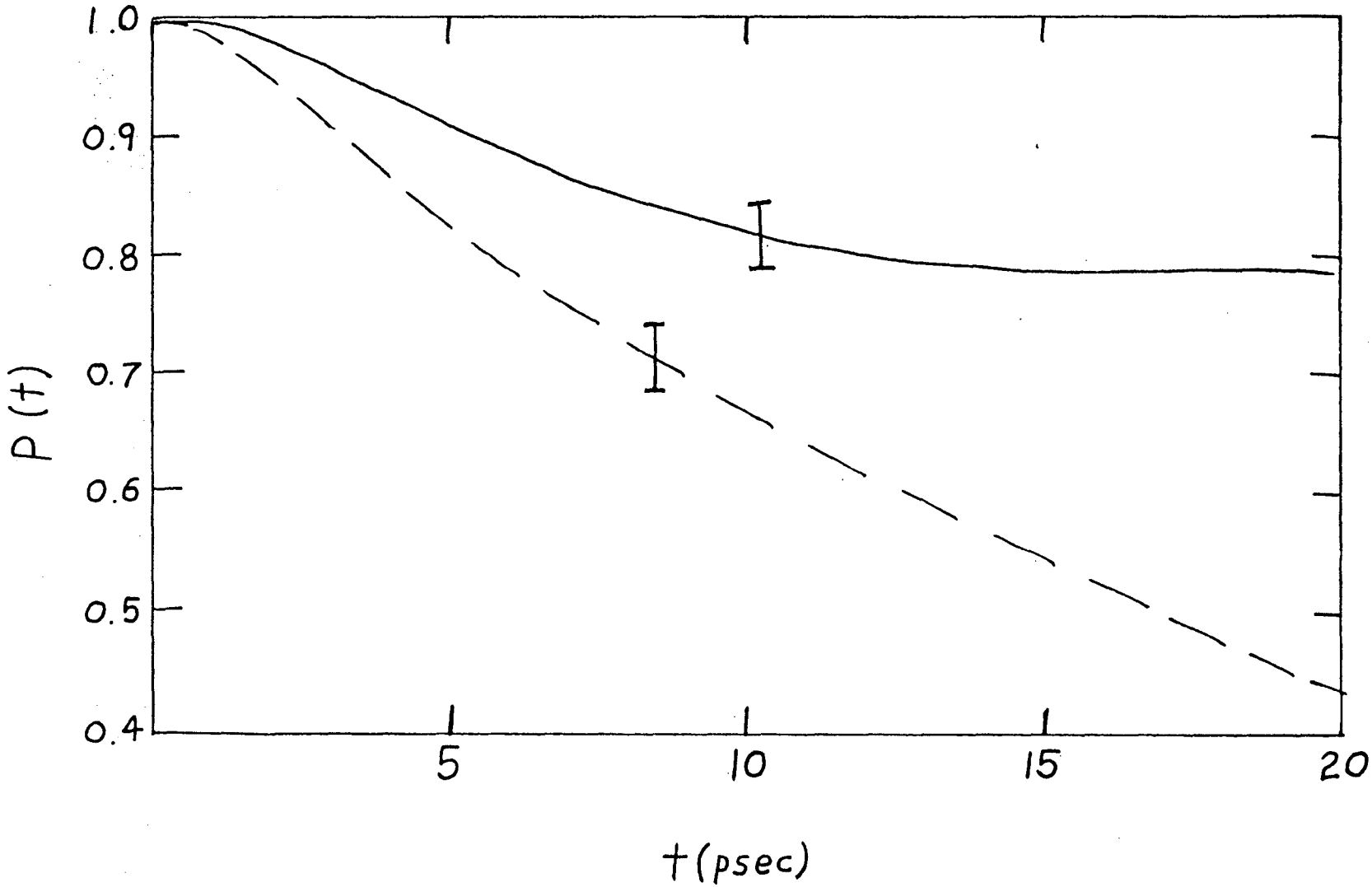

This report was done with support from the Department of Energy. Any conclusions or opinions expressed in this report represent solely those of the author(s) and not necessarily those of The Regents of the University of California, the Lawrence Berkeley Laboratory or the Department of Energy.

Reference to a company or product name does not imply approval or recommendation of the product by the University of California or the U.S. Department of Energy to the exclusion of others that may be suitable.

TECHNICAL INFORMATION DEPARTMENT
LAWRENCE BERKELEY LABORATORY
UNIVERSITY OF CALIFORNIA
BERKELEY, CALIFORNIA 94720